

Results from Shell Model Monte Carlo Studies

S. E. Koonin

Kellogg Radiation Laboratory, 106-38
California Institute of Technology, Pasadena, CA 91125 USA

D. J. Dean

Physics Division, Oak Ridge National Laboratory,
Oak Ridge, TN 37831-6373 USA

K. Langanke

Institute for Physics and Astronomy, Aarhus University, Denmark

KEY WORDS: Nuclei, Shell Model, Monte Carlo

Abstract

We review results obtained using Shell Model Monte Carlo (SMMC) techniques. These methods reduce the imaginary-time many-body evolution operator to a coherent superposition of one-body evolutions in fluctuating one-body fields; the resultant path integral is evaluated stochastically. After a brief review of the methods, we discuss a variety of nuclear physics applications. These include studies of the ground-state properties of pf -shell nuclei, Gamow-Teller strength distributions, thermal and rotational pairing properties of nuclei near $N = Z$, γ -soft nuclei, and $\beta\beta$ -decay in ^{76}Ge . Several other illustrative calculations are also reviewed. Finally, we discuss prospects for further progress in SMMC and related calculations.

Contents

1	Introduction	2
2	Methods	4
2.1	Observables	4
2.2	The Hubbard-Stratonovich transformation	7
2.3	Monte Carlo quadrature and the sign problem	8
2.4	Computational considerations	13

3	Results	15
3.1	Ground state properties of medium mass nuclei	15
3.1.1	<i>pf</i> -shell nuclei	15
3.1.2	The $0f_{5/2}1p0g_{9/2}$ model space	17
3.1.3	Gamow-Teller strengths and distributions	19
3.2	Pair correlations	22
3.2.1	Ground state pair correlations	24
3.2.2	Pairing and rotation	27
3.2.3	Pairing and temperature	28
3.3	$\beta\beta$ -decay	33
3.4	γ -soft nuclei	37
4	Illustrative calculations	43
4.1	Giant dipole resonances	43
4.2	Multi-major shell calculations	43
5	Concluding remarks	45

1 Introduction

The notion of independent particles moving in a common one-body potential is central to our description of atoms, metals, and hadrons. It is also realized in nuclei, and the shell structure associated with the magic numbers was first put on a firm basis in 1949, when the magic numbers were explained by an harmonic oscillator spectrum with a strong, inverted (with respect to the atomic case) spin-orbit potential [1].

But nuclei differ from the other quantal systems cited above in that the residual interaction between the valence fermions is strong and so severely perturbs the naive single-particle picture. This interaction mixes together many different configurations to produce the true eigenstates and, because of its coherence, there emerge phenomena such as pairing, modification of sum rules, deformation, and collective rotations and vibrations. An accurate treatment of the residual interaction is therefore essential to properly describe nuclei.

A hierarchy of models has been developed to treat various aspects of the mean field and correlations; Skyrme Hartree-Fock[2] for the mean field, Hartree-Fock Bogolioubov for the pairing correlations [3], and RPA [4] for particle-hole correlations. But short of a complete solution of the

many-body problem, the shell model is regarded as the most fundamental approach for studying nuclear structure, provided that the single-particle space in which calculations are performed is large enough. Success was demonstrated early in the $0p$ -shell [5], in the $0s$ - $1d$ [6], in the $0f_{7/2}$ region [7], and more recently in the $1p0f$ -shell using interactions developed by Kuo and Brown [8] and modified by Zuker and Poves [9].

The traditional numerical approach to the nuclear shell model is to diagonalize the hamiltonian matrix within a limited many-body basis [10]. Direct diagonalization gives the wave functions which can then be used to calculate the properties of specific levels. The shell model treated in this way has been quite successful in describing sd -shell nuclei [11], and has also been used to successfully describe various properties of the lower pf -shell [12, 13]. However, the direct-diagonalization procedure is limited by memory requirements that grow combinatorially with the size of the single-particle space, N_s , and with the number of valance particles, N_v . In the pf -shell where ^{40}Ca is the core, the largest systematic study thus far treats $A = 48, 49$ [12], an achievement that required approximately five generations of technological and software improvement.

To circumvent the limitations of direct diagonalization, we have proposed an alternative treatment of the shell model [14, 15, 16, 17, 18]. Our methods are based on a path-integral formulation of the imaginary-time many-body propagator, $\exp(-\beta H)$, where H is the shell model hamiltonian, and β is the reciprocal of the temperature. We employ the Hubbard-Stratonovich (HS) transformation [19] to recast the two-body terms in the exponential into one-body terms with an integration over auxiliary fields. Thus the nucleons are seen as independent particles moving about in fluctuating fields [20]. Such auxiliary field methods have also been applied to condensed matter systems such as the Hubbard model [21, 22], yielding important information about electron correlations and magnetic properties.

Having circumvented the diagonalization of the hamiltonian, we are left with a large multidimensional integration to perform, for which we use the Monte Carlo sampling techniques of Metropolis *et al* [23]. Realistic nuclear hamiltonians often have a sign problem that hampers the Monte Carlo quadrature. We have overcome this by an extrapolation procedure from a family of hamiltonians, all of which have no sign problem and are close to the full hamiltonian. It is important to note that these calculations are carried out on large scale parallel computers, a technology that is essential to implement these methods.

In this article, we briefly outline SMMC methods in Section II, then

concentrate our discussion on the physics results obtained. We discuss in Section III our major results, which include ground state properties of *pf*-shell nuclei, Gamow-Teller strengths and distributions, thermal and rotational pairing properties of nuclei near $N = Z$, γ -soft nuclei, and $\beta\beta$ -decay. In Section IV, several other illustrative studies are reviewed. We conclude in Section V with a discussion of future prospects. Our coverage of the field extends through February 1997.

2 Methods

The nuclear shell model is defined by a set of spin-orbit coupled single-particle states with quantum numbers ljm denoting the orbital angular momentum (l) and the total angular momenta (j) and its z -component, m . Although non-spherical one-body potentials are a common efficiency used in describing deformed nuclei, for the rotationally invariant hamiltonians used in SMMC so far, these states have energies ε_{lj} that are independent of m . The single-particle states and energies may be different for neutrons and protons, in which case it is convenient to include also the isospin component $t_3 = \pm 1/2$ in the state description. We will use the label α for the set of quantum numbers ljm or $ljmt_3$, as appropriate.

In the following we briefly outline the formalism of the SMMC method. We begin with a brief description of statistical mechanics techniques used in our approach, then discuss the Hubbard-Stratonovich transformation, and end with a discussion of Monte Carlo sampling procedures. We refer the reader to previous works [15, 18] for a more detailed exposition.

2.1 Observables

SMMC methods rely on an ability to calculate the imaginary-time many-body evolution operator, $\exp(-\beta H)$, where β is a real c -number. The many-body hamiltonian can be written schematically as

$$H = \varepsilon \mathcal{O} + \frac{1}{2} V \mathcal{O} \mathcal{O}, \quad (1)$$

where \mathcal{O} is a density operator, V is the strength of the two-body interaction, and ε a single-particle energy. In the full problem, there are many such quantities with various orbital indices that are summed over, but we omit them here for the sake of clarity.

While the SMMC technique does not result in a complete solution to the many-body problem in the sense of giving all eigenvalues and eigenstates of H , it can result in much useful information. For example, the expectation value of some observable Ω can be obtained by calculating

$$\langle \Omega \rangle = \frac{\text{Tr} e^{-\beta H} \Omega}{\text{Tr} e^{-\beta H}}. \quad (2)$$

Here, $\beta \equiv T^{-1}$ is interpreted as the inverse of the temperature T , and the many-body trace is defined as

$$\text{Tr} X \equiv \sum_i \langle i | X | i \rangle, \quad (3)$$

where the sum is over many-body states of the system. In the canonical ensemble, this sum is over all states with a specified number of nucleons (implemented by “number projection” [15, 18]), while the grand canonical ensemble introduces a chemical potential and sums over *all* many-body states.

In the limit of low temperature ($T \rightarrow 0$ or $\beta \rightarrow \infty$), the canonical trace reduces to a ground state expectation value. Alternatively, if $|\Phi\rangle$ is a many-body trial state not orthogonal to the exact ground state, $|\Psi\rangle$, then $e^{-\beta H}$ can be used as a filter to refine $|\Phi\rangle$ to $|\Psi\rangle$ as β becomes large. An observable can be calculated in this “zero temperature” method as

$$\frac{\langle \Phi | e^{-\frac{\beta}{2} H} \Omega e^{-\frac{\beta}{2} H} | \Phi \rangle}{\langle \Phi | e^{-\beta H} | \Phi \rangle} \xrightarrow{\beta \rightarrow \infty} \frac{\langle \Psi | \Omega | \Psi \rangle}{\langle \Psi | \Psi \rangle}. \quad (4)$$

If Ω is the hamiltonian, then (4) at $\beta = 0$ is the variational estimate of the energy, and improves as β increases. Of course, the efficiency of the refinement for any observable depends upon the degree to which $|\Phi\rangle$ approximates $|\Psi\rangle$.

Beyond such static properties, $e^{-\beta H}$ allows us to obtain some information about the dynamical response of the system. For an operator Ω , the response function $R_\Omega(\tau)$ in the canonical ensemble is defined as

$$R_\Omega(\tau) \equiv \frac{\text{Tr} e^{-(\beta-\tau)H} \Omega^\dagger e^{-\tau H} \Omega}{\text{Tr} e^{-\beta H}} \equiv \langle \Omega^\dagger(\tau) \Omega(0) \rangle, \quad (5)$$

where $\Omega^\dagger(\tau) \equiv e^{\tau H} \Omega^\dagger e^{-\tau H}$ is the imaginary-time Heisenberg operator. Interesting choices for Ω are the annihilation operators for particular orbitals, the Gamow-Teller, $M1$, or quadrupole moment, etc. Inserting

complete sets of A -body eigenstates of H ($\{|i\rangle, |f\rangle\}$) with energies $E_{i,f}$ shows that

$$R_\Omega(\tau) = \frac{1}{Z} \sum_{if} e^{-\beta E_i} |\langle f|\Omega|i\rangle|^2 e^{-\tau(E_f - E_i)}, \quad (6)$$

where $Z = \sum_i e^{-\beta E_i}$ is the partition function. Thus, $R_\Omega(\tau)$ is the Laplace transform of the strength function $S_\Omega(E)$:

$$R_\Omega(\tau) = \int_{-\infty}^{\infty} e^{-\tau E} S_\Omega(E) dE; \quad (7)$$

$$S_\Omega(E) = \frac{1}{Z} \sum_{fi} e^{-\beta E_i} |\langle f|\Omega|i\rangle|^2 \delta(E - E_f + E_i). \quad (8)$$

Hence, if we can calculate $R_\Omega(\tau)$, $S_\Omega(E)$ can be determined. Short of a full inversion of the Laplace transform (which is often numerically difficult), the behavior of $R_\Omega(\tau)$ for small τ gives information about the energy-weighted moments of S_Ω . In particular,

$$R_\Omega(0) = \int_{-\infty}^{\infty} S_\Omega(E) dE = \frac{1}{Z} \sum_i e^{-\beta E_i} |\langle f|\Omega|i\rangle|^2 = \langle \Omega^\dagger \Omega \rangle_A \quad (9)$$

is the total strength,

$$-R'_\Omega(0) = \int_{-\infty}^{\infty} S_\Omega(E) E dE = \frac{1}{Z} \sum_{if} e^{-\beta E_i} |\langle f|\Omega|i\rangle|^2 (E_f - E_i) \quad (10)$$

is the first moment (the prime denotes differentiation with respect to τ).

It is important to note that we usually cannot obtain detailed spectroscopic information from SMMC calculations. Rather, we can calculate expectation values of operators in the thermodynamic ensembles or the ground state. Occasionally, these can indirectly furnish properties of excited states. For example, if there is a collective 2^+ state absorbing most of the $E2$ strength, then the centroid of the quadrupole response function will be a good estimate of its energy. But, in general, we are without the numerous specific excitation energies and wavefunctions that characterize a direct diagonalization. This is both a blessing and a curse. The former is that for the very large model spaces of interest, there is no way in which we can deal explicitly with all of the wavefunctions and excitation energies. Indeed, we often don't need to, as experiments only measure average nuclear properties at a given excitation energy. The curse is that comparison with detailed properties of

specific levels is difficult. In this sense, the SMMC method is complementary to direct diagonalization for modest model spaces, but is the only method for treating very large problems.

2.2 The Hubbard-Stratonovich transformation

It remains to describe the Hubbard-Stratonovich “trick” by which $e^{-\beta H}$ is managed. In broad terms, the difficult many-body evolution is replaced by a superposition of an infinity of tractable one-body evolutions, each in a different external field, σ . Integration over the external fields then reduces the many-body problem to quadrature.

To illustrate the approach, let us assume that only one operator \mathcal{O} appears in the hamiltonian (1). Then all of the difficulty arises from the two-body interaction, that term in H quadratic in \mathcal{O} . If H were solely linear in \mathcal{O} , we would have a one-body quantum system, which is readily dealt with. To linearize the evolution, we employ the Gaussian identity

$$e^{-\beta H} = \sqrt{\frac{\beta |V|}{2\pi}} \int_{-\infty}^{\infty} d\sigma e^{-\frac{1}{2}\beta|V|\sigma^2} e^{-\beta h}; \quad h = \epsilon\mathcal{O} + sV\sigma\mathcal{O}. \quad (11)$$

Here, h is a one-body operator associated with a c -number field σ , and the many-body evolution is obtained by integrating the one-body evolution $U_\sigma \equiv e^{-\beta h}$ over all σ with a Gaussian weight. The phase, s , is 1 if $V < 0$ or i if $V > 0$. Equation (11) is easily verified by completing the square in the exponent of the integrand; since we have assumed that there is only a single operator \mathcal{O} , there is no need to worry about non-commutation.

For a realistic hamiltonian, there will be many non-commuting density operators \mathcal{O}_α present, but we can always reduce the two-body term to diagonal form. Thus for a general two-body interaction in a general time-reversal invariant form, we write

$$H = \sum_{\alpha} (\epsilon_{\alpha}^* \bar{\mathcal{O}}_{\alpha} + \epsilon_{\alpha} \mathcal{O}_{\alpha}) + \frac{1}{2} \sum_{\alpha} V_{\alpha} \{ \mathcal{O}_{\alpha}, \bar{\mathcal{O}}_{\alpha} \}, \quad (12)$$

where $\bar{\mathcal{O}}_{\alpha}$ is the time reverse of \mathcal{O}_{α} . Since, in general, $[\mathcal{O}_{\alpha}, \mathcal{O}_{\beta}] \neq 0$, we must split the interval β into N_t “time slices” of length $\Delta\beta \equiv \beta/N_t$,

$$e^{-\beta H} = [e^{-\Delta\beta H}]^{N_t}, \quad (13)$$

and for each time slice $n = 1, \dots, N_t$ perform a linearization similar to Eq. 11 using auxiliary fields $\sigma_{\alpha n}$. Note that because the various

\mathcal{O}_α need not commute, the representation of $e^{-\Delta\beta h}$ must be accurate through order $(\Delta\beta)^2$ to achieve an overall accuracy of order $\Delta\beta$.

We are now able to write expressions for observables as the ratio of two field integrals. Thus expectations of observables can be written as

$$\langle \Omega \rangle = \frac{\int \mathcal{D}\sigma W_\sigma \Omega_\sigma}{\int \mathcal{D}\sigma W_\sigma}, \quad (14)$$

where

$$W_\sigma = G_\sigma \text{Tr} U_\sigma; \quad G_\sigma = e^{-\Delta\beta \sum_{\alpha n} |V_\alpha| |\sigma_{\alpha n}|^2};$$

$$\Omega_\sigma = \frac{\text{Tr} U_\sigma \Omega}{\text{Tr} U_\sigma}; \quad \mathcal{D}\sigma \equiv \prod_{n=1}^{N_t} \prod_{\alpha} d\sigma_{\alpha n} d\sigma_{\alpha n}^* \left(\frac{\Delta\beta |V_\alpha|}{2\pi} \right), \quad (15)$$

and

$$U_\sigma = U_{N_t} \dots U_2 U_1; \quad U_n = e^{-\Delta\beta h_n};$$

$$h_n = \sum_{\alpha} (\varepsilon_\alpha^* + s_\alpha V_\alpha \sigma_{\alpha n}) \bar{\mathcal{O}}_\alpha + (\varepsilon_\alpha + s_\alpha V_\alpha \sigma_{\alpha n}^*) \mathcal{O}_\alpha. \quad (16)$$

This is, of course, a discrete version of a path integral over σ . Because there is a field variable for each operator at each time slice, the dimension of the integrals $\mathcal{D}\sigma$ can be very large, often exceeding 10^5 . The errors in Eq. 14 are of order $\Delta\beta$, so that high accuracy requires large N_t and perhaps extrapolation to $N_t = \infty$ ($\Delta\beta = 0$).

Thus, the many-body observable is the weighted average (weight W_σ) of the observable Ω_σ calculated in an ensemble involving only the one-body evolution U_σ . Similar expressions involving two σ fields (one each for $e^{-\tau H}$ and $e^{-(\beta-\tau)H}$) can be written down for the response function (5), and all are readily adapted to the canonical or grand canonical ensembles or to the zero-temperature case.

An expression of the form (14) has a number of attractive features. First, the problem has been reduced to quadrature—we need only calculate the ratio of two integrals. Second, all of the quantum mechanics (which appears in Ω_σ) is of the one-body variety, which is simply handled by the algebra of $N_s \times N_s$ matrices. The price to pay is that we must treat the one-body problem for all possible σ fields.

2.3 Monte Carlo quadrature and the sign problem

The manipulations of the previous sections have reduced the shell model to quadrature. That is, thermodynamic expectation values are given as the ratio of two multidimensional integrals over the auxiliary fields. The dimension D of these integrals is of order $N_s^2 N_t$, which can exceed

10^5 for the problems of interest. Monte Carlo methods are the only practical means of evaluating such integrals. In this section, we review those aspects of Monte Carlo quadrature relevant to the task at hand.

We begin by recasting the ratio of integrals in Eq. (14) as

$$\langle \Omega \rangle = \int d^D \sigma P_\sigma \Omega_\sigma, \quad (17)$$

where

$$P_\sigma = \frac{W_\sigma}{\int d^D \sigma W_\sigma}. \quad (18)$$

Since $\int d^D \sigma P_\sigma = 1$ and $P_\sigma \geq 0$, we can think of P_σ as a probability density and $\langle \Omega \rangle$ as the average of Ω_σ weighted by P_σ . Thus, if $\{\sigma_s, s = 1, \dots, S\}$ are a set of S field configurations randomly chosen with probability density P_σ , we can approximate $\langle \Omega \rangle$ as

$$\langle \Omega \rangle \approx \frac{1}{S} \sum_{s=1}^S \Omega_s, \quad (19)$$

where Ω_s is the value of Ω_σ at the field configuration σ_s . Since this estimate of $\langle \Omega \rangle$ depends upon the randomly chosen field configurations, it too will be a random variable whose average value is the required integral. To quantify the uncertainty of this estimate, we consider each of the Ω_s as a random variable and invoke the central limit theorem to obtain

$$\sigma_{\langle \Omega \rangle}^2 = \frac{1}{S} \int d^D \sigma P_\sigma (\Omega_\sigma - \langle \Omega \rangle)^2 \approx \frac{1}{S^2} \sum_{s=1}^S (\Omega_s - \langle \Omega \rangle)^2. \quad (20)$$

This variance varies as $S^{-1/2}$.

We employ the Metropolis, Rosenbluth, Rosenbluth, Teller, and Teller algorithm [23], to generate the field configurations \mathcal{O}_s , which requires only the ability to calculate the weight function for a given value of the integration variables. This method requires that the weight function W_σ must be real and non-negative. Unfortunately, many of the hamiltonians of physical interest suffer from a sign problem, in that W_σ is negative over significant fractions of the integration volume. To understand the implications of this, let us rewrite Eq. (17) as

$$\langle \Omega \rangle = \int d^D \sigma P_\sigma \Phi_\sigma \Omega_\sigma, \quad (21)$$

where

$$P_\sigma = \frac{|W_\sigma|}{\int d^D\sigma |W_\sigma| \Phi_\sigma},$$

and $\Phi_\sigma = W_\sigma / |W_\sigma|$ is the sign of the real part of W_σ . (Note that since the partition function is real, we can neglect the imaginary part.) Since $|W_\sigma|$ is non-negative by definition, we can interpret it, suitably normalized, as a probability density, so that upon rewriting (17) as

$$\langle \Omega \rangle = \frac{\int d\sigma |W_\sigma| \Phi_\sigma \Omega_\sigma}{\int d\sigma |W_\sigma| \Phi_\sigma} = \frac{\langle \Phi \Omega \rangle}{\langle \Phi \rangle}, \quad (22)$$

we can think of the observable as a ratio in which the numerator and denominator can be separately evaluated by MC quadrature. Leaving aside the issue of correlations between estimates of these two quantities (they can always be evaluated using separate Metropolis walks), the fractional variance of $\langle \Omega \rangle$ will be

$$\frac{\sigma_\Omega}{\langle \Omega \rangle} = \sqrt{\frac{\langle \Omega^2 \rangle}{\langle \Phi \Omega \rangle^2} + \frac{1}{\langle \Phi \rangle^2} - 2}, \quad (23)$$

which becomes unacceptably large as the average sign $\langle \Phi \rangle$ approaches zero. The average sign of the weight thus determines the feasibility of naive MC quadrature. In most cases $\langle \Phi \rangle$ decreases exponentially with β or with the number of time slices [24].

It has been shown [15] that for even-even and $N = Z$ nuclei there is no sign problem for hamiltonians if all $V_\alpha \leq 0$. Such forces include reasonable approximations to the realistic hamiltonian like pairing plus multipole interactions. However, for an arbitrary hamiltonian, we are not guaranteed that all $V_\alpha \leq 0$ (see for example [17, 15]). However, we may expect that a *realistic* hamiltonian will be dominated by terms like those of the schematic pairing plus multipole force (which is, after all, why the schematic forces were developed) so that it is, in some sense, close to a hamiltonian for which the MC is directly applicable. Thus, the “practical solution” to the sign problem presented in Ref. [17] is based on an extrapolation of observables calculated for a “nearby” family of hamiltonians whose integrands have a positive sign. Success depends crucially upon the degree of extrapolation required. Empirically, one finds that, for all of the many realistic interactions tested in the *sd*- and *pf*-shells, the extrapolation required is modest, amounting to a factor-of-two variation in the isovector monopole pairing strength.

Based on the above observation, it is possible to decompose H in Eq. 12 into its “good” and “bad” parts, $H = H_G + H_B$, with

$$\begin{aligned} H_G &= \sum_{\alpha} (\epsilon_{\alpha}^* \bar{\mathcal{O}}_{\alpha} + \epsilon_{\alpha} \mathcal{O}_{\alpha}) + \frac{1}{2} \sum_{V_{\alpha} < 0} V_{\alpha} \{ \mathcal{O}_{\alpha}, \bar{\mathcal{O}}_{\alpha} \} \\ H_B &= \frac{1}{2} \sum_{V_{\alpha} > 0} V_{\alpha} \{ \mathcal{O}_{\alpha}, \bar{\mathcal{O}}_{\alpha} \}. \end{aligned} \quad (24)$$

The “good” hamiltonian H_G includes, in addition to the one-body terms, all the two-body interactions with $V_{\alpha} \leq 0$, while the “bad” hamiltonian H_B contains all interactions with $V_{\alpha} > 0$. By construction, calculations with H_G alone have $\Phi_{\sigma} \equiv 1$ and are thus free of the sign problem.

We define a family of hamiltonians H_g that depend on a continuous real parameter g as $H_g = f(g)H_G + gH_B$, so that $H_{g=1} = H$, and $f(g)$ is a function with $f(1) = 1$ and $f(g < 0) > 0$ that can be chosen to make the extrapolations less severe. (In practical applications $f(g) = 1 - (1 - g)/\chi$ with $\chi \approx 4$ has been found to be a good choice.) If the V_{α} that are large in magnitude are “good,” we expect that $H_{g=0} = H_G$ is a reasonable starting point for the calculation of an observable $\langle \Omega \rangle$. One might then hope to calculate $\langle \Omega \rangle_g = \text{Tr}(\Omega e^{-\beta H_g}) / \text{Tr}(e^{-\beta H_g})$ for small $g > 0$ and then to extrapolate to $g = 1$, but typically $\langle \Phi \rangle$ collapses even for small positive g . However, it is evident from our construction that H_g is characterized by $\Phi_{\sigma} \equiv 1$ for any $g \leq 0$, since all the “bad” $V_{\alpha} (> 0)$ are replaced by “good” $gV_{\alpha} < 0$. We can therefore calculate $\langle \Omega \rangle_g$ for any $g \leq 0$ by a Monte Carlo sampling that is free of the sign problem. If $\langle \Omega \rangle_g$ is a smooth function of g , it should then be possible to extrapolate to $g = 1$ (i.e., to the original hamiltonian) from $g \leq 0$. We emphasize that $g = 0$ is not expected to be a singular point of $\langle \Omega \rangle_g$; it is special only in the Monte Carlo evaluation.

In Fig. 2.3 we exemplify the g -extrapolation procedure for several observables calculated for ^{54}Fe . In all cases we use polynomial extrapolations from negative g -values to the physical case, $g = 1$. The degree of the polynomial is usually chosen to be the smallest that yields a χ^2 per degree of freedom less than 1. However, in several studies, like the one of the pf -shell nuclei reported in Section III, we have conservatively chosen second-order polynomials for all extrapolations, although in many cases a first-order polynomial already resulted in χ^2 -values less than 1. At $T = 0$ the variational principle requires that $\langle H \rangle$ has a minimum at $g = 1$. We have incorporated this fact in our extrapolations of ground state energies by using a second-order polynomial with zero-derivative at $g = 1$.

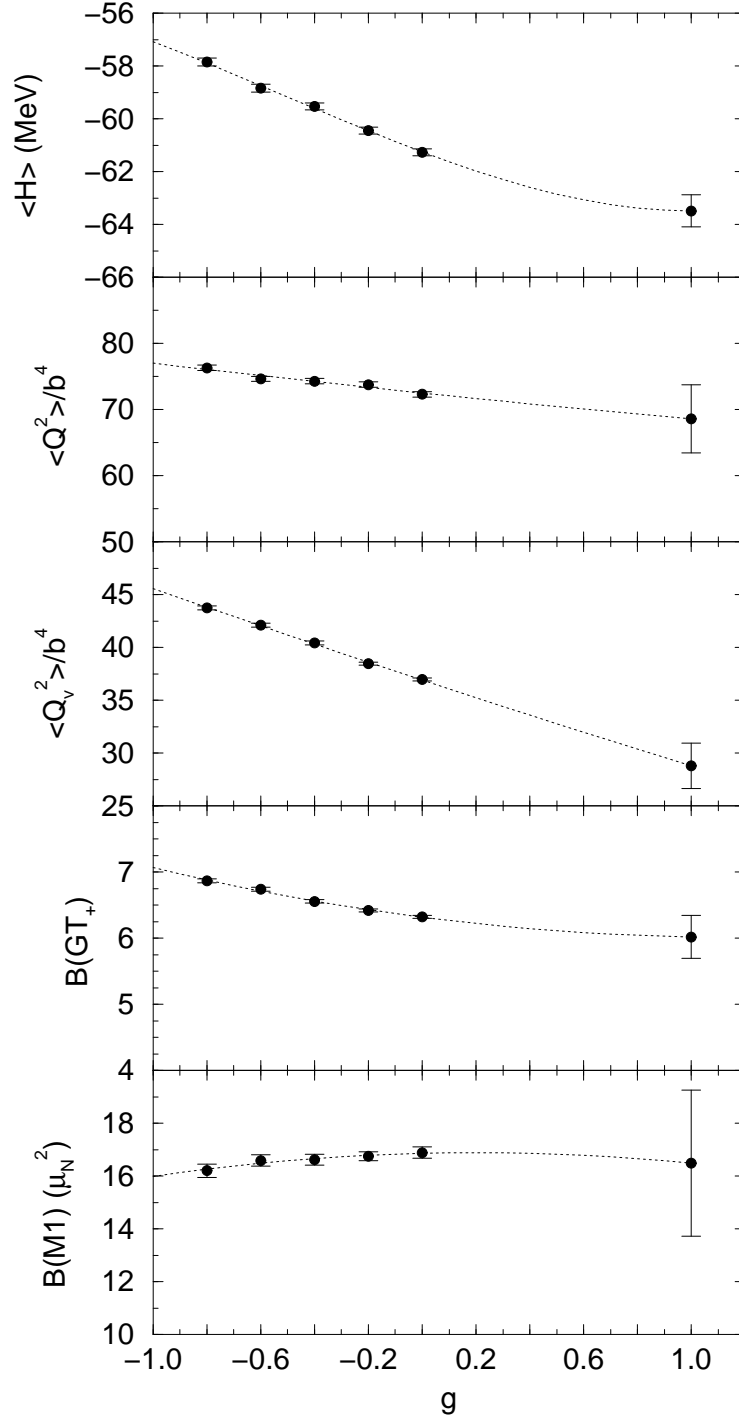


Fig 2.3. g -extrapolation of several observables for ^{54}Fe calculated with the Kuo-Brown interaction KB3.

2.4 Computational considerations

The present SMMC code is roughly the fourth major revision of a program whose development began in late 1990 with a single-species, single- j -shell version. It is now a modular package of some 10,000 commented lines of FORTRAN. All floating point computations are double precision (64-bit).

The package performs all of the functions necessary for shell model Monte Carlo calculations: initialization, thermalization of the Metropolis walk, generation of the Monte Carlo samples, evaluation of static observables and response functions (canonical or grand-canonical), Maximum Entropy extraction of strength functions [18], and the extrapolation in g required to solve the sign problem, as discussed in section 2.3. The data input and results output use standard shell model conventions, so that it is easy to change the two-body matrix elements of the interaction to incorporate additional one- or two-body observables in the analysis, or to add or change the orbitals in the calculation. The code has been de-bugged and tested extensively against direct diagonalization results in the sd - and lower pf -shells. Its operation by an experienced user can be described as “routine,” although it takes several weeks to acquire that experience.

Shell model Monte Carlo calculations are extraordinarily well-suited to Multiple Instruction/Multiple Data (MIMD) architectures. Very few problems are encountered in porting to a new machine, and the operation generally takes less than a day. Indeed, our code is “embarrassingly parallel”: separate Metropolis random walks are started on each computational node, which then produces a specified number of Monte Carlo samples at regular intervals during the walk. Data from all of the nodes are sent to a central node for evaluation of the Monte Carlo averages and their uncertainties.

To date, we have implemented the parallel version of our code on the Intel DELTA and PARAGON machines at Caltech and ORNL (each with 512 i860 processors), on the 128-processor IBM SP-1 at ANL, the 512-processor IBM SP-2 at Maui, and on a Fujitsu VPP500 shared-memory vector processor (24 CPU’s). In all cases, the ratio of communications to computation is very low, with efficiencies always greater than 95%.

Table 1 shows benchmarks of our code on various single processors. The test calculation involved a canonical ensemble in the full pf -shell ($N_s = 20$ for each type of nucleon, implying 20×20 matrices) using a realistic interaction. $N_t = 32$ time slices were used at $\beta = 2 \text{ MeV}^{-1}$

Processor	Peak MF	Average MF	Samples/hr.
i860	35	9	44
IBM-SP2 Thin66	56	36	179
ALPHA-400	56	28	141

Table 1: Benchmarks of the SMMC code in various processors.

$0p$	6
$1s-0d$	12
$1p-0f$	20
$1p-0f-0g_{9/2}$	30
$2s-1d-0g$	30
$2p-1f-0g_{9/2}-0i_{13/2}$	44

Table 2: Matrix dimension for various model spaces.

($\Delta\beta = 0.0625 \text{ MeV}^{-1}$). Thirty static observables and seven dynamical response functions were calculated at a single g -value (see section 7). Note that the computational speed is independent of the interaction and of the number of nucleons occupying the shell. Beyond using library subroutines (BLAS and LAPACK routines), no attempt was made to optimize the assembly level code in any of these cases. Approximately 40% of the computational effort is in matrix-multiply operations. A significant remainder of the effort goes into building the one-body hamiltonian (13%), setting up the one-body evolution operators (15%), and calculating two-body observables (15%), none of which is easily vectorizable. In general, the computation time scales as $N_s^3 N_t$, and is spent roughly equally on the dynamical response functions and the static observable sampling.

The memory required for our calculations scales as $\bar{N}_s^2 N_t$. \bar{N}_s^2 is the average of the squares of the numbers of neutron and proton single-particle states. Sample values of N_s for one isospin type are shown for various model spaces in Table 2.

The code is currently structured so that a calculation with $\bar{N}_s = 32$, six j -orbitals, and $N_t = 64$ time slices will fit in 12 MB of memory. A calculation in the $(1p-0f)$ - $(2s-1d-0g)$ basis has $\bar{N}_s = 50$ and would require about 64 MB of memory for $N_t = 64$ time slices and about

128 MB for $N_t = 128$.

3 Results

In the past four years SMMC techniques have been applied in a variety of ways to nuclei in the pf -shell and other regions using realistic or semi-realistic interactions. In this section we will detail several of the important results of these calculations. These are, broadly, ground state and thermal properties of iron region nuclei, nuclear pair correlations, $\beta\beta$ -decay, and γ -soft studies.

3.1 Ground state properties of medium mass nuclei

3.1.1 pf -shell nuclei

While complete $0\hbar\omega$ calculations can be carried out by direct diagonalization in the p - and sd -shells, the exponentially increasing number of configurations limits such studies in the next (pf) shell to only the very lightest nuclei [25, 12]. SMMC techniques allow calculation of ground-state observables in the full $0\hbar\omega$ model space for nuclei throughout the pf -shell. Here, we discuss a set of such calculations that uses the modified KB3 interaction [9]; the single-particle basis is such that $N_s = 20$ for both protons and neutrons. These studies were performed for 28 even-even Ti, Cr, Fe, Ni, and Zn isotopes and 4 odd-odd $N = Z$ nuclei. A more detailed description of the calculations and their results are found in Ref. [26].

Figure 3.1.1 shows systematic results for the mass defects obtained directly from $\langle H \rangle$. The SMMC results have been corrected for the coulomb energy, which is not included in the KB3 interaction, using [12]

$$H_{\text{Coul}} = \frac{\pi(\pi - 1)}{2} \cdot 0.35 - \pi\nu 0.05 + \pi \cdot 7.289. \quad (25)$$

where π and ν are the numbers of valence protons and neutrons, respectively, and the energy is in MeV. As in Ref. [12], we have increased the calculated energy expectation values by $0.014 \cdot n(n - 1)$ MeV (where $n = \pi + \nu$ is the number of valence nucleons) to correct for a “tiny” residual monopole defect in the KB3 interaction. In general, there is excellent agreement; the average error for the nuclei shown is +0.45 MeV, which agrees roughly with the internal excitation energy of a few hundred keV expected in our finite-temperature calculation.

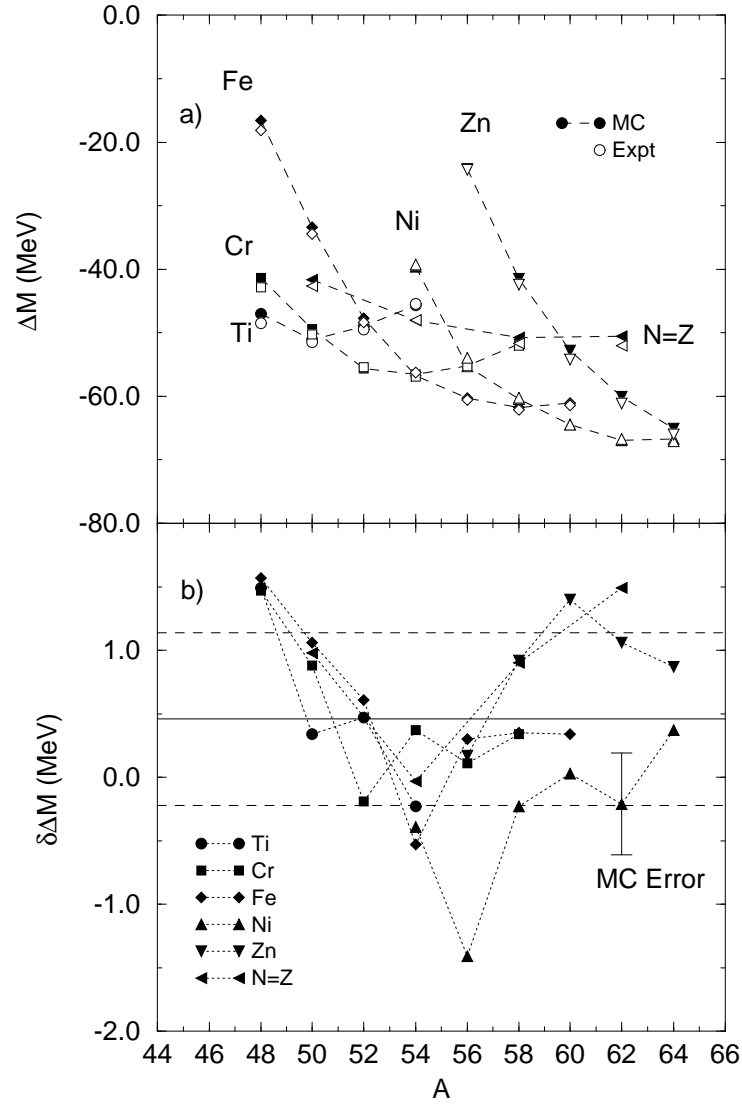


FIG 3.1.1 Upper panel (a): Comparison of the mass excesses ΔM as calculated within the SMMC approach with data. Lower panel (b): Discrepancy between the SMMC results for the mass excesses and the data, $\delta\Delta M$. The solid line shows the average discrepancy, 450 keV, while the dashed lines show the rms variation about this value (from [26]).

Figure 3.1.1 shows the calculated total $E2$ strengths for selected pf -shell nuclei. This quantity is defined as

$$B(E2) = \langle (e_p Q_p + e_n Q_n)^2 \rangle, \quad (26)$$

with

$$Q_{p(n)} = \sum_i r_i^2 Y_2(\theta_i, \phi_i), \quad (27)$$

where the sum runs over all valence protons (neutrons). The effective charges were chosen to be $e_p = 1.35$ and $e_n = 0.35$, while we used $b = 1.01A^{1/6}$ fm for the oscillator length. Shown for comparison are the $B(E2)$ values for the $0_1^+ \rightarrow 2_1^+$ transition in each nucleus; in even-even nuclei some 20-30% of the strength comes from higher transitions. The overall trend is well reproduced. For the nickel isotopes $^{58,60,64}\text{Ni}$, the total $B(E2)$ strength is known from (e, e') data and agrees very nicely with our SMMC results.

3.1.2 The $0f_{5/2}1p0g_{9/2}$ model space

In order to investigate heavier systems, the $0g_{9/2}$ was included in the pf model space[8]. However, we found that the coupling between the $0f_{7/2}$ and $0g_{9/2}$ orbitals causes significant center-of-mass contamination to the ground state, and we therefore close the $0f_{7/2}$. The model space is thus $0f_{5/2}1p0g_{9/2}$. This appears to be a good approximation in systems where N and Z are greater than 28. The monopole terms of this new interaction were modified [27] to give a good description of the spectra of nuclei in the Ni isotopes. Since ^{56}Ni is the core of this model space, the single-particle energies were determined from the ^{57}Ni spectrum.

Shell-model masses must be corrected for coulomb effects and for ‘grand-monopole’ terms [28] that are not taken into account when determining interaction matrix elements from nuclear spectra. Following Ref. [12] we have fitted a correction to the calculated binding energies which takes into account the coulomb energy and residual effects of the monopole terms. The form of this correction is

$$H_c = \alpha\pi(\pi - 1) + \beta\pi\nu + \gamma\pi + \delta n(n - 1) + \varepsilon n \quad (28)$$

where π, ν are the number of valence protons and neutrons, and $n = \pi + \nu$, and all parameters are in units of MeV. γ is held fixed at 7.289. Minimizing χ^2 for the difference between experimental and theoretical binding energies relative to the ^{56}Ni core gives $\alpha = 0.234$, $\beta = 0.0156$, $\delta = 0.0316$, and $\varepsilon = 1.828$.

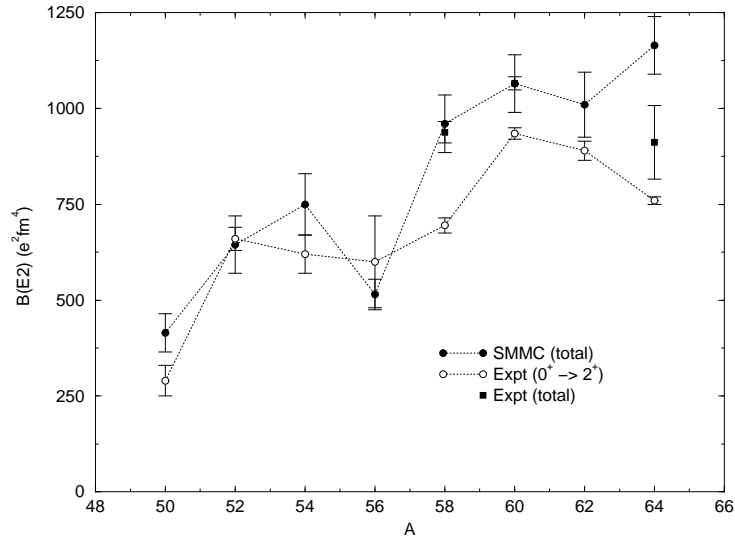


FIG 3.1.1 Comparison of the experimental $B(E2, 0_1^+ \rightarrow 2_1^+)$ strengths with the total $B(E2)$ strength calculated in the SMMC approach for various pf -shell nuclei having either a proton or neutron number of 28. For the nickel isotopes $^{58,60,64}\text{Ni}$ the total $B(E2)$ strength (full squares) is known from inelastic electron scattering data (from [26]).

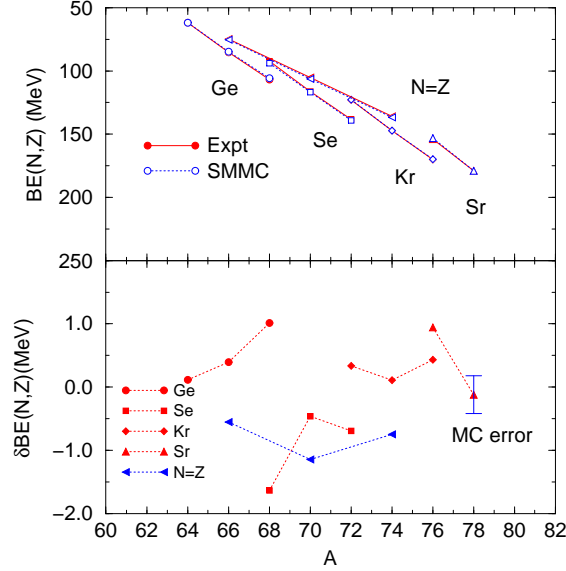


FIG 3.1.2. Calculated mass excesses for nuclei in the mass range $A = 64$ – 80 are compared with experiment (top panel), and the difference between experiment and theory is shown (bottom panel).

Shown in Fig. 3.1.2 are the experimental and theoretical binding energies $BE(N, Z)$ for the nuclei studied here (top panel), and the difference between experiment and theory (bottom panel). The overall agreement is reasonable.

3.1.3 Gamow-Teller strengths and distributions

The Gamow-Teller (GT) properties of nuclei in this region of the periodic table are crucial for supernova physics [29]. The core of a massive star at the end of hydrostatic burning is stabilized by electron degeneracy pressure as long as its mass does not exceed the appropriate Chandrasekhar mass M_{CH} . If the core mass exceeds M_{CH} , electrons are captured by nuclei [29]. For many of the nuclei that determine the elec-

tron capture rate in this early stage of the presupernova [30], Gamow-Teller (GT) transitions contribute significantly to the electron capture rate. Due to insufficient experimental information, the GT_+ transition rates have so far been treated only qualitatively in presupernova collapse simulations, assuming the GT_+ strength to reside in a single resonance whose energy relative to the daughter ground state has been parametrized phenomenologically [31]; the total GT_+ strength has been taken from the single particle model. Recent (n, p) experiments [32]-[36], however, show that the GT_+ strength is fragmented over many states, while the total strength is significantly quenched compared to the single particle model. (A recent update of the GT_+ rates for use in supernova simulations assumed a constant quenching factor of 2 [30].)

The total GT strengths are defined as

$$B(GT_{\pm}) = \langle (\vec{\sigma}\tau_{\pm})^2 \rangle. \quad (29)$$

From $0\hbar\omega$ shell model studies of the GT strengths for sd shell nuclei and for light pf shell nuclei it has been deduced that the spin operator in (31) should be replaced by an effective one, $\vec{\sigma}_{\text{eff}} = \vec{\sigma}/1.26$ [6, 12]. This renormalization is not well understood. It is believed to be related either to a second-order core polarization caused by the tensor force [37], or to the screening of the Gamow-Teller operator by Δ -hole pairs [38]. Using the effective spin operator, our calculated $B(GT_+)$ are in excellent agreement with the data deduced from (n, p) reactions (Figure 3.1.3). Thus, our calculations support both the statement that the spin operator is renormalized by a universal factor (1/1.26) in nuclei, and the statement that complete shell-model calculations can account for the GT strength observed experimentally.

In a series of truncated shell-model calculations, Aufderheide and collaborators have demonstrated that a strong phase space dependence makes the Gamow-Teller contributions to the presupernova electron capture rates more sensitive to the strength *distribution* in the daughter nucleus than to the total strength [39]. In this work it also became apparent that complete $0\hbar\omega$ studies of the GT_+ strength distribution are desirable. Such studies are now possible using the SMMC approach.

To determine the GT_+ strength distribution, we have calculated the response function of the $\sigma\tau_+$ operator, $R_{GT}(\tau)$, as defined in Eq. (5). As the strength function $S_{GT}(E)$ is the inverse Laplace transform of $R_{GT}(\tau)$, we have used the Maximum Entropy technique, described in Ref. [18], to extract $S_{GT}(E)$.

As first examples we have studied several nuclei (^{51}V , $^{54,56}\text{Fe}$, ^{55}Mn , $^{58,60,62,64}\text{Ni}$, and ^{59}Co), for which the Gamow-Teller strength distribu-

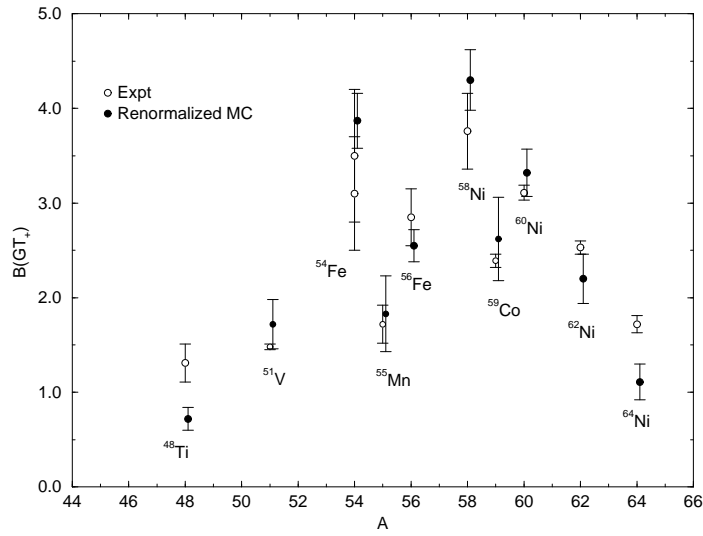


FIG 3.1.3. Comparison of the renormalized total Gamow-Teller strength, as calculated within the present SMMC approach, and the experimental $B(GT_+)$ values deduced from (n, p) data [32]-[36]. [For the odd nuclei (^{51}V , ^{55}Mn and ^{59}Co) the SMMC calculations have been performed at $\beta = 1 \text{ MeV}^{-1}$ to avoid the odd- A sign problem. For even-even nuclei the GT strength calculated at this temperature is still a good approximation for the ground state value, as discussed in the text.]

tion in the daughter nucleus is known from (n, p) experiments [32]-[36]. However, note that electron capture by these nuclei plays only a minor role in the presupernova collapse. As SMMC calculates the strength function within the parent nucleus, the results have been shifted using the experimental Q -values, and the Coulomb correction has been performed using Eq. (25). For all nuclei, the SMMC approach calculates the centroid and width of the strength distribution in good agreement with data (see Fig. 3.1.3). The centroid of the GT_+ strength distributions is found to be nearly independent of temperature, while its width increases with temperature.

Following the formalism described in Refs. [31, 30], the Gamow-Teller contributions to the electron capture rates under typical presupernova conditions have been calculated, assuming that the electrons have a Fermi-Dirac distribution with a chemical potential adopted from the stellar trajectory at the electron-to-nucleon ratio corresponding to the particular nucleus [30]. The calculations have been performed using both the SMMC and experimental GT_+ strength distributions [32]-[36]. The two electron capture rates agree within a factor of two for temperatures $T = (3 - 5) \times 10^9$ Kelvin, which is the relevant temperature regime in the presupernova collapse [30]. Thus, for the first time it is possible to calculate, with reasonable accuracy, the electron capture rate for nuclei like ^{55}Co or ^{56}Ni , which dominate the electron capture process in the early presupernova collapse [30].

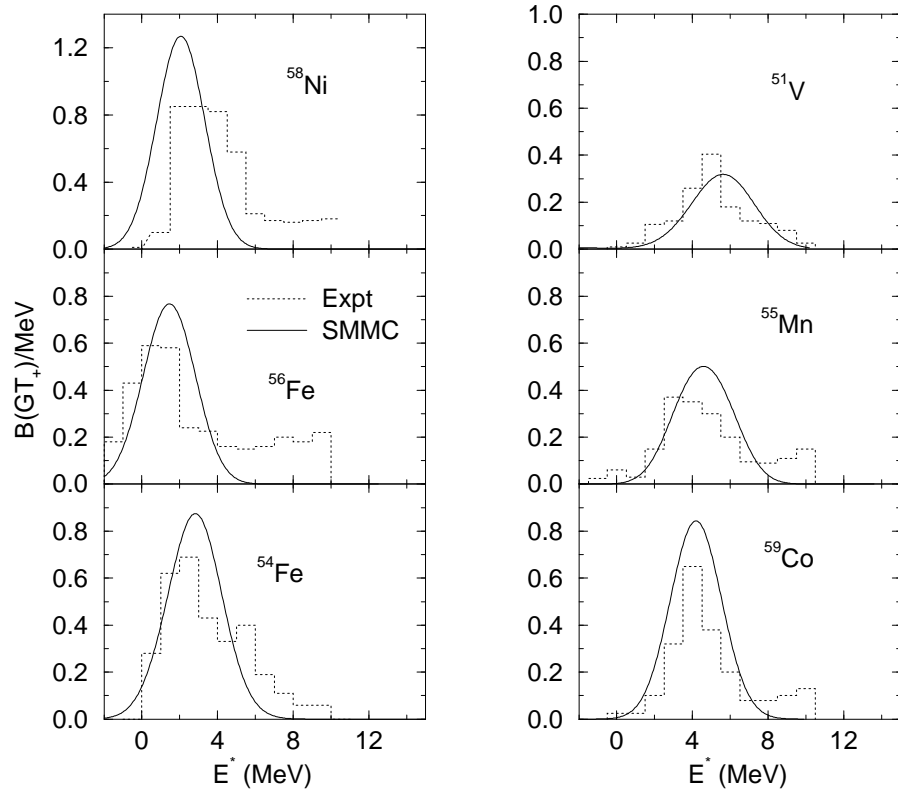
3.2 Pair correlations

The residual nuclear interaction builds up pairing correlations in a nucleus. Introducing nucleon creation operators a^\dagger , these correlations can be studied by defining pair creation operators

$$A_{JM}^\dagger(j_a j_b) = \frac{1}{\sqrt{1 + \delta_{ab}}} [a_{j_a}^\dagger \times a_{j_b}^\dagger]_{JM} \quad (30)$$

for proton-proton or neutron-neutron pairs, and

$$A_{JM}^\dagger(j_a j_b) = \frac{1}{\sqrt{2(1 + \delta_{ab})}} \left\{ [a_{p j_a}^\dagger \times a_{n j_b}^\dagger]_{JM} \right. \\ \left. \pm [a_{n j_a}^\dagger \times a_{p j_b}^\dagger]_{JM} \right\}, \quad (31)$$



. FIG 3.1.3. Shown are SMMC GT_+ strength distributions (solid line) for various nuclei in the iron region. The energies refer to the daughter nuclei. The dashed histograms show the experimental strength distribution as extracted from (n, p) data. (Following [13] the calculated strength distributions have been folded with Gaussians of width 1.77 MeV to account for the experimental resolution.)

for proton-neutron pairs where “+(-)” is for $T = 0(T = 1)$ pn -pairing. With these definitions, we construct a pair matrix

$$M_{\alpha\alpha'}^J = \sum_M \langle A_{JM}^\dagger(j_a, j_b) A_{JM}(j_c, j_d) \rangle, \quad (32)$$

where $\alpha = \{j_a, j_b\}$ and $\alpha' = \{j_c, j_d\}$ and the expectation value is in the ground state or canonical ensemble at a prescribed temperature. The pairing strength for a given J is then given by

$$P(J) = \sum_{\alpha \geq \alpha'} M_{\alpha, \alpha'}^J. \quad (33)$$

An alternative measure of the overall pair correlations is given in terms of the BCS pair operator

$$\Delta_{JM}^\dagger = \sum_\alpha A_{JM}^\dagger(\alpha). \quad (34)$$

The quantity $\sum_M \langle \Delta_{JM}^\dagger \Delta_{JM} \rangle$ is then a measure of the number of nucleon pairs with spin J . For the results discussed below, the BCS-like definition for the overall pairing strength yields the same qualitative results for the pairing content as the definition (33). Some SMMC results for BCS pairing in nuclei $A = 48 - 60$ are published in Refs. [26, 40, 41, 42].

With our definition in (33) the pairing strength is positive at the mean-field level. The mean-field pairing strength, $P_{\text{MF}}(J)$, can be defined by replacing the expectation values of the two-body matrix elements in the definition of M^J by

$$\langle a_1^\dagger a_2^\dagger a_3 a_4 \rangle \rightarrow n_1 n_2 (\delta_{13} \delta_{24} - \delta_{23} \delta_{14}), \quad (35)$$

where $n_k = \langle a_k^\dagger a_k \rangle$ is the occupation number of the orbital k . This mean-field value provides a baseline against which true pair correlations can be judged, by defining

$$P_{\text{cor}}(J) = P(J) - P_{\text{MF}}(J). \quad (36)$$

3.2.1 Ground state pair correlations

In a first project we studied the pair correlations in several even-even pf shell nuclei ($^{54,56,58}\text{Fe}$ and ^{56}Cr) [40]. As expected, we found a large excess of $J = 0^+$ like-particle pairing in the ground states of these nuclei. With increasing temperature, these pairing correlations decrease

and at around $T = 1$ MeV the like-particle pairs break in these nuclei (pairing phase transition). Our calculations also indicate that isoscalar proton-neutron (mainly $J = 1^+$) pairs persist to higher temperatures. In Ref. [40] we have related the thermal dependence of several observables to the temperature dependence of associated pairing correlations.

It has long been anticipated that $J = 0^+$ proton-neutron correlations play an important role in the ground states of $N = Z$ nuclei. These correlations were explored with SMMC for $N = Z$ nuclei with $A = 48 - 58$ in the pf -shell [41], and $A = 64 - 74$ in the $0f_{5/2}1p0g_{9/2}$ space. As the even-even $N = Z$ nuclei have isospin $T = 0$, $\langle A^\dagger A \rangle$ is identical in all three isovector 0^+ pairing channels. This symmetry does not hold for the odd-odd $N = Z$ nuclei in this mass region, which usually have $T = 1$ ground states, and $\langle A^\dagger A \rangle$ can differ for proton-neutron and like-nucleon pairs. (The expectation values for proton pairs and neutron pairs are identical.)

We find the proton-neutron pairing strength is significantly larger for odd-odd $N = Z$ nuclei than in even-even nuclei, while the 0^+ proton and neutron pairing shows the opposite behavior, in both cases leading to a noticeable odd-even staggering, as displayed in Fig. 3.2.1 for the pf shell. Due to the strong pairing in the $f_{7/2}$ orbital, all three isovector 0^+ channels of the pairing matrix exhibit essentially only one large eigenvalue which is used as a convenient measure of the pairing strength in Fig. 3.2.1. This staggering is caused by a constructive (destructive) interference of the isotensor and isoscalar parts of $A^\dagger A$ in the odd-odd (even-even) $N = Z$ nuclei. The isoscalar part is related to the pairing energy and is roughly constant for the nuclei we have studied.

Fig. 3.2.1 shows the correlated pairs for $N = Z$ nuclei in the $A = 64 - 74$ region of the $0f_{5/2}1p0g_{9/2}$ space. The correlated pairs exhibit a strong $J = 0, T = 1$ like-particle staggering for the even-even and odd-odd $N = Z$ systems, while the number of correlated proton-neutron pairs is much larger than the like-particle number for the odd-odd systems. The correlated pairing behavior of $N = Z, N = Z + 2, N = Z + 4$ nuclei is shown in Fig. 3.2.1, where one clearly sees the decrease in $T=1$ proton-neutron pairing as one moves away from $N = Z$. As discussed by Engel *et al.* [42], increasing the number of neutron pairs increases the collectivity of the neutron condensate, making fewer neutrons available to pair with protons. As a result, the protons pair more often with one another, although their number has not changed, and the np pairing drops drastically. A weak neutron shell closure is evident in the Kr isotopes as the neutrons fill to $N=40$ at ^{76}Kr . Although the neutron pairing correlations decrease here, they are not zero as the $g_{9/2}$ has

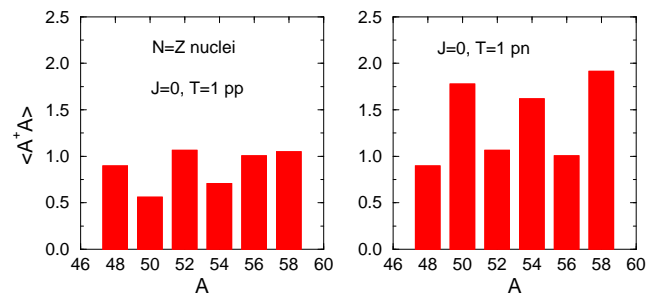


Fig 3.2.1. Largest eigenvalues for the $J = 0$, $T = 1$ proton-proton (left) and proton-neutron (right) pairing matrix as a function of mass number.

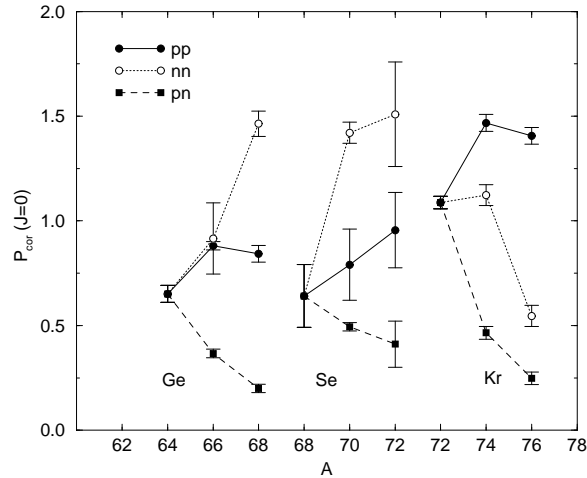


Fig 3.2.1. Correlated $J = 0$, $T = 1$ pairs in the proton-proton and proton-neutron channels for selected isotope chains in the $0f_{5/2}1p0g_{9/2}$ model space.

some occupation.

3.2.2 Pairing and rotation

A recent study [43] of the γ decays of the odd-odd $N = Z$ nucleus ^{74}Rb revealed the phenomenon of an isospin band crossing at modest excitation energies. While the ground state rotational band can be identified as being formed from the $T = 1$ isobaric analogue states of ^{74}Kr , a $T = 0$ band becomes energetically favored over the $T = 1$ band with increasing rotational frequency. To study this isospin band crossing, we have performed a cranked SMMC calculation [44] in which the shell model hamiltonian is replaced by $H \rightarrow H + \omega J_z$. Note that since J_z is a time-odd operator, the sign problem is reintroduced, and good statistical sampling imposes a limit on ω . For the calculations presented in Table 3, the largest cranking frequency was $\omega = 0.4$ MeV. In agreement with experiment, we find $T = 1$ for the ground state ($\omega = 0$). How-

ever, with increasing frequency $T = 0$ states are mixed in (and even dominate at large angular momenta) and $\langle T^2 \rangle$ decreases, as can be seen in Table 3. Thus our calculation confirms that ^{74}Rb changes from a $T = 1$ dominated system to one dominated by $T = 0$ states with increasing rotational frequency. To understand the apparent crossing of the $T = 1$ and $T = 0$ bands, we have studied the various pair correlations as a function of rotational frequency. We find that the isovector $J = 0$ correlations and the aligned isoscalar $J = 9$ pn correlations are most important in this transition. These correlations are plotted in Fig. 3.2.2 as a function of $\langle J_z \rangle$, where we have defined pair correlations by Eq. (36). Strikingly, the largest pair correlations are found in the isovector $J = 0$ and isoscalar $J = 9$ proton-neutron channels at low and high frequencies, respectively. Furthermore, the variation of isospin with increasing frequency reflects the relative strengths of these two pn correlations. Our calculation clearly confirms that proton-neutron correlations determine the behavior of the odd-odd $N = Z$ nucleus ^{74}Rb , as already supposed in [43].

With increasing frequency, the isovector $J = 0$ pn correlations decrease rapidly to a constant at $\langle J_z \rangle \approx 3$. This behavior is accompanied by an increase of the pn correlations in the maximally aligned channel, $J = 9, T = 0$ which dominates ^{74}Rb at rotational frequencies where the $J = 0$ pn correlations become small. Furthermore, although $J = 8, T = 1$ pairs exist, they do not exhibit correlations beyond the mean field, as shown in Fig. 3.2.2. We note that the experiment also indicates that the mixing of $T = 0$ states sets in near $J = 3$.

3.2.3 Pairing and temperature

Another striking difference in proton-neutron pairing can be found in the thermal properties of odd-odd (e.g. ^{50}Mn) and even-even (e.g. ^{52}Fe) $N = Z$ nuclei [41]. As in other even-even $N = Z$ nuclei, the ground state isospin of ^{52}Fe is $T = 0$ and isospin symmetry forces pp , nn , and np pairing to be identical. With increasing temperature, $T = 1$ components are slowly mixed in, breaking the symmetry between nn - pp and np pairing. However, $\langle T^2 \rangle \approx 0$ for $T < 1$ MeV and the symmetry holds. As $J = 0^+$ pairs break at around this temperature in even-even nuclei in this mass range, the phase transition is clearly noticeable in all three isovector pairing channels.

As discussed above, the ground state of the odd-odd nucleus ^{50}Mn (with isospin $T = 1$) is dominated by 0^+ pn correlations. As a striking feature shown in Fig. 3.2.3, the proton-neutron pairing decreases rapidly

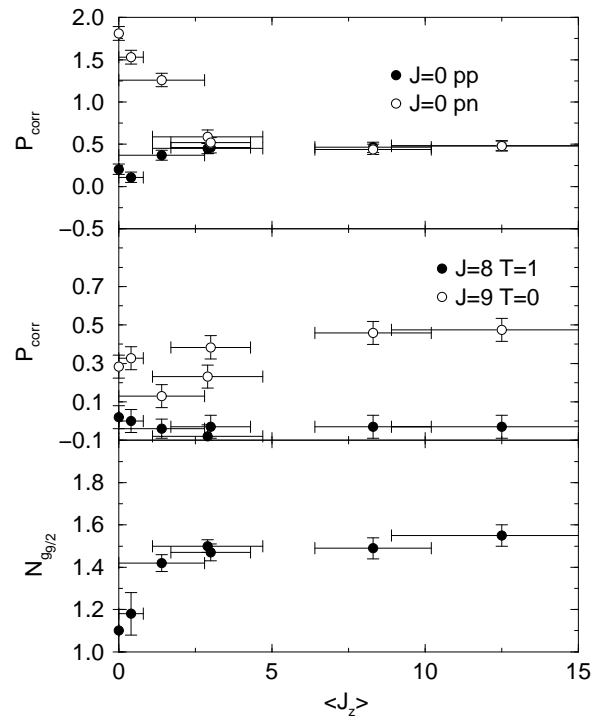


Fig 3.2.2. Selected pair correlations and the proton $g_{9/2}$ occupation number (bottom panel) as a function of $\langle J_z \rangle$. The top panel shows the isovector $J = 0$ pp and pn correlations, while the isoscalar $J = 9$ and isovector $J = 8$ pn correlations are shown in the middle panel.

Table 3: Summary of various properties of ^{74}Rb . These results, quoted as a function of the cranking frequency ω , include $\sqrt{\langle J^2 \rangle}$, $\langle T^2 \rangle$, the proton-proton $J = 0$ pairing correlations ($J = 0, pp$), $J = 0, T = 1, pn$ pairing correlations ($J = 0, pn$).

ω MeV	$\sqrt{\langle J^2 \rangle}$	$\langle T^2 \rangle$	$J = 0$ pp	$J = 0$ pn
0.00	3.5 ± 0.6	1.97 ± 0.05	0.21 ± 0.05	1.81 ± 0.08
0.10	2.1 ± 0.9	1.825 ± 0.03	0.11 ± 0.05	1.53 ± 0.08
0.20	2.9 ± 0.7	1.98 ± 0.10	0.37 ± 0.06	1.26 ± 0.08
0.25	2.6 ± 1.1	1.72 ± 0.16	0.45 ± 0.06	0.60 ± 0.08
0.30	3.3 ± 0.8	1.77 ± 0.13	0.46 ± 0.06	0.52 ± 0.08
0.35	6.6 ± 3.1	1.40 ± 0.14	0.46 ± 0.06	0.44 ± 0.08
0.40	11.3 ± 1.9	0.69 ± 0.20	0.48 ± 0.06	0.48 ± 0.08

with temperature and has dropped to the mean-field value by $T \sim 0.75$ MeV, while the like-particle pairing remains roughly constant to 1.1 MeV. The vanishing of the pn correlations is accompanied by a change in isospin, which decreases from the ground state value $\langle T^2 \rangle = 2$ to $\langle T^2 \rangle \approx 0.2$ at temperatures near $T = 1$ MeV.

As required by general thermodynamic principles, the internal energy increases steadily with temperature. The heat capacity $C(T) = dE/dT$, with $E = \langle H \rangle$, is usually associated with the level density parameter a by $C(T) = 2a(T)T$. As is typical for even-even nuclei [45] $a(T)$ increases from $a = 0$ at $T=0$ to a roughly constant value at temperatures above the phase transition. We find $a(T) \approx 5.3 \pm 1.2$ MeV $^{-1}$ at $T \geq 1$ MeV, in agreement with the empirical value of 6.5 MeV $^{-1}$ [46] for ^{52}Fe . At higher temperatures, $a(T)$ must decrease due to the finite model space of our calculation.

The temperature dependence of E in ^{50}Mn is significantly different from that in even-even nuclei. As can be seen in Fig. 3.2.3, E increases approximately linearly with temperature, corresponding to a constant heat capacity $C(T) \approx 5.4 \pm 1$ MeV $^{-1}$; the level density parameter decreases like $a(T) \sim T^{-1}$ in the temperature interval between 0.4 MeV and 1.5 MeV. We note that the same linear increase of the energy with temperature is observed in SMMC studies of odd-odd $N = Z$ nuclei performed with a pairing+quadrupole hamiltonian [47].

To investigate the apparent differences in the thermal behavior of even-even and odd-odd $N = Z$ nuclei in a more systematic way, we

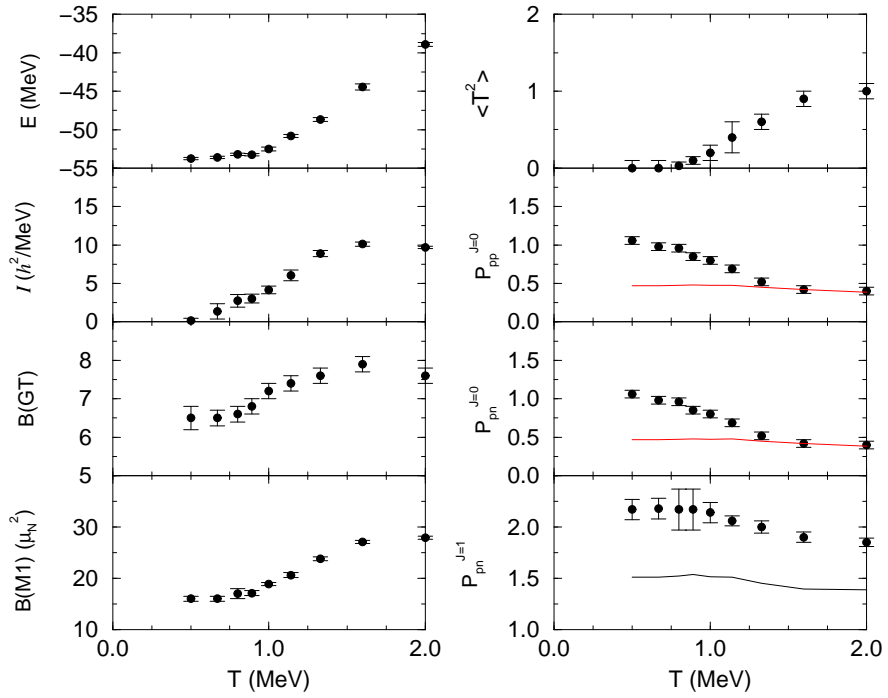


Fig. 3.2.3. Thermal properties of ^{52}Fe . The SMMC results are shown with error bars, while the lines indicate the mean-field values for the respective pair correlations.

have performed SMMC calculations for ^{50}Mn and ^{50}Cr using a pairing+quadrupole hamiltonian. Note that the quadrupole part allows for $T = 0$ pn correlations. The strength of the quadrupole component has been adjusted to reasonably reproduce SMMC results for the realistic KB3 interaction. This hamiltonian has no sign problem, thus significantly reducing the statistical uncertainties (and also potential systematic errors related to the g-extrapolation). Despite its simplicity, the hamiltonian nevertheless embraces much of the essential degrees of freedom governing the thermal response at low temperatures.

The ground states of ^{50}Cr and ^{50}Mn belong to the same $T = 1$ multiplet and are therefore isobaric analogues. This is correctly recovered in the SMMC calculation as the energy expectation values at low temperatures are, within error bars, identical. However, $\langle T^2 \rangle = 1.89 \pm 0.07$ for ^{50}Mn at $T = 0.33$ MeV (the lowest temperature at which we have performed these SMMC calculations) indicates some isoscalar components being mixed in. (Experimentally, the lowest $T = 0$ state in ^{50}Mn is at an excitation energy of 0.2 MeV.) With increasing temperature the relative strength of the isovector component in ^{50}Mn weakens. Correspondingly, $\langle T^2 \rangle$ decreases to 1.34 ± 0.04 at $T = 0.8$ MeV. As isospin $T = 0$ states cannot be formed in ^{50}Cr due to the neutron excess ($\langle T^2 \rangle = 2.1$ at $T = 0.8$ MeV), this nucleus has fewer degrees of freedom than ^{50}Mn . As a consequence ^{50}Mn has a higher excitation energy, or relatedly a higher level density, than ^{50}Cr at modest temperatures (at $T = 0.8$ MeV $\langle H \rangle = -7.55 \pm 0.13$ MeV for ^{50}Mn and -8.28 ± 0.08 MeV for ^{50}Cr). At even higher temperatures, the like-particle correlations break (see Fig. 3.2.3). For both nuclei, isospin states with $T \geq 2$ get mixed in and $\langle T^2 \rangle$ increases. For temperatures above the phase transition ($T \geq 1$ MeV), the thermal properties for both nuclei ($H, J^2, Q^2, Q_v^2, Q_p^2, Q_n^2$; the latter two with the appropriate scaling by the proton and neutron numbers) become almost the same. At $T \leq 1$ MeV, the isovector 0^+ pairing correlations behave as for the realistic KB3 interaction. In particular, there is the noticeable excess of pp and nn correlations in the even-even nucleus ^{50}Cr at low temperatures, while the odd-odd ^{50}Mn is dominated by pn correlations. The latter decrease rather rapidly with temperature, while the pp and nn correlations in ^{50}Cr show the behavior characteristic of a phase transition near 1 MeV, which is typical for even-even nuclei in this mass range studied with the KB3 interaction.

However, there are a few differences between calculations with the simple hamiltonian and the realistic one. First, for the simple hamiltonian all isovector correlations decrease much more slowly at temper-

atures exceeding 1 MeV. The origin for this is the missing isoscalar pn correlations, which dominate nuclear properties at $T \geq 1$ MeV [41]. Their persistence at these higher temperatures further suppresses the isovector correlations when the realistic hamiltonian is used. Second, quantities that are sensitive to np correlations are not correctly described by the simple hamiltonian. Among these are the Gamow-Teller strengths. Here the realistic hamiltonian yields $B(GT_+) = 5.2 \pm 1.8$ for ^{50}Mn and 2.2 ± 0.2 for ^{50}Cr (after the renormalization of the spin operator). In contrast, for the simple hamiltonian we find $B(GT_+) = 4.5 \pm 0.1$ for ^{50}Mn and 3.8 ± 0.01 for ^{50}Cr . These values have to be compared with the independent-particle model estimates: 6.9 (^{50}Mn) and 5.1 (^{50}Cr). While the large error bars make a comparison for ^{50}Mn meaningless, the isovector pn pairing accounts for somewhat less than half of the GT_+ quenching in ^{50}Cr , the reminder being due to isoscalar pn correlations between spin-orbit partners, introduced by the $(\vec{\sigma}\tau)^2$ piece missing in the simple hamiltonian. Third, the level density at moderate temperatures ($T \approx 1$ MeV) is less for the realistic hamiltonian than for the simple one; one of the reasons again is the missing isoscalar pn correlations that push levels to higher energies.

Nevertheless these SMMC calculations with the sign-problem-free hamiltonian are quite illustrative and can be extended to odd- A and odd-odd $N \neq Z$ nuclei. First calculations show that one can investigate these nuclei down to temperatures of order 0.5 MeV, before the sign-problem seriously enters again.

3.3 $\beta\beta$ -decay

The second-order weak process $(Z, A) \rightarrow (Z + 2, A) + 2e^- + 2\bar{\nu}_e$ is an important “background” to searches for the lepton-number violating neutrinoless mode, $(Z, A) \rightarrow (Z + 2, A)$. The calculation of the nuclear matrix element for these two processes is a challenging problem in nuclear structure, and has been done in a full pf model space for only the lightest of several candidates, ^{48}Ca . P.B. Radha *et al.* have performed first Monte Carlo calculations of the 2ν $\beta\beta$ matrix elements in very large model spaces [48].

In two-neutrino double β -decay, the nuclear matrix element of interest is

$$M^{2\nu} \equiv \sum_m \frac{\langle f_0 | \mathbf{G} | m \rangle \cdot \langle m | \mathbf{G} | i_0 \rangle}{E_m - \Omega}, \quad (37)$$

where $|i_0\rangle$ and $|f_0\rangle$ are the 0^+ ground states of the initial and final even-

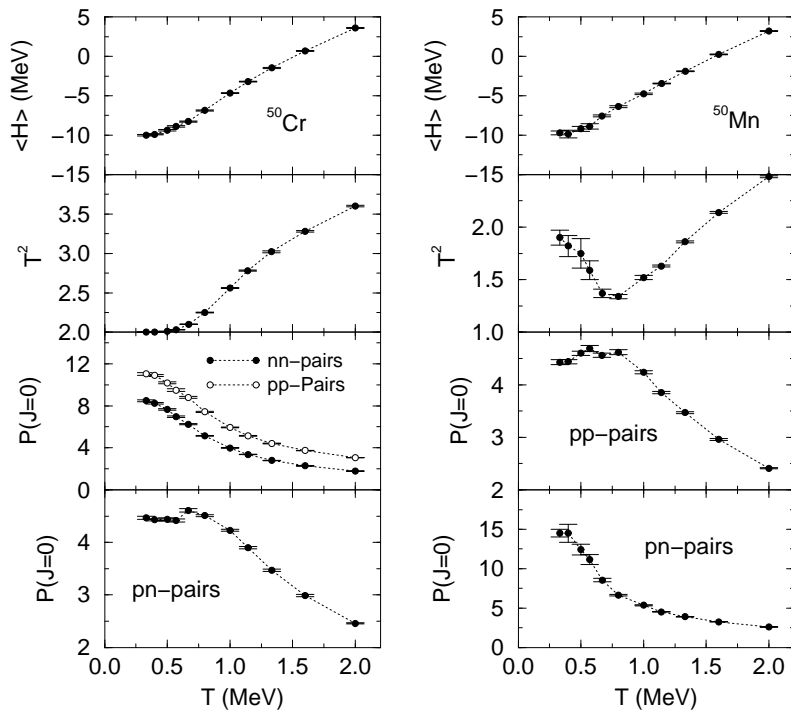


Fig. 3.2.3. Thermal properties of ^{50}Cr (left) and ^{50}Mn (right) calculated with a simple pairing + quadrupole hamiltonian.

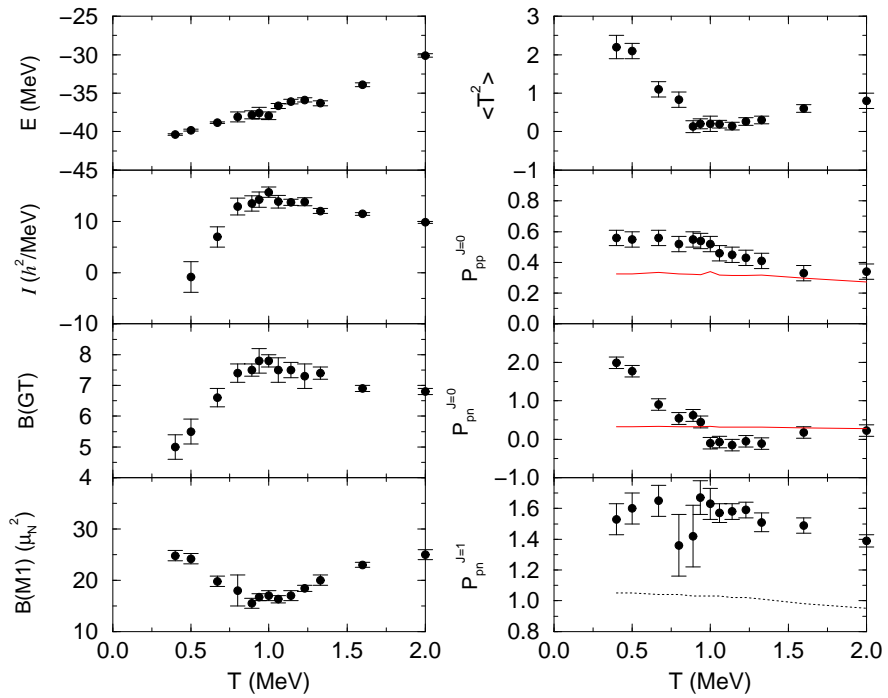


Fig. 3.2.3. Thermal properties of ^{50}Mn . The SMMC results are shown with error bars, while the lines indicate the mean-field values for the respective pair correlations.

even nuclei, and $|m\rangle$ is a 1^+ state of the intermediate odd-odd nucleus; the sum is over all such states. In this expression, $\mathbf{G} = \sigma\tau_-$ is the Gamow-Teller operator for β^- -decay (i.e., that which changes a neutron into a proton) and $\Omega = (E_{i_0} + E_{f_0})/2$. A common approximation to $M^{2\nu}$ is the closure value,

$$M^{2\nu} = \frac{M_c}{\bar{E}} \quad (38)$$

where \bar{E} is an average energy dominator and

$$M_c \equiv \sum_m \langle f_0 | \mathbf{G} | m \rangle \langle m | \mathbf{G} | i_0 \rangle = \langle f_0 | \mathbf{G} \cdot \mathbf{G} | i_0 \rangle. \quad (39)$$

SMMC methods can be used to calculate both M_c and $M^{2\nu}$. To do so, consider the function

$$\begin{aligned} \phi(\tau, \tau') &= \langle e^{H(\tau+\tau')} \mathbf{G}^\dagger \cdot \mathbf{G}^\dagger e^{-H\tau} \mathbf{G} e^{-H\tau'} \mathbf{G} \rangle \\ &= \frac{1}{Z} \text{Tr}_A \left[e^{-(\beta-\tau-\tau')H} \mathbf{G}^\dagger \cdot \mathbf{G}^\dagger e^{-\tau H} \mathbf{G} e^{-\tau' H} \mathbf{G} \right], \quad (40) \end{aligned}$$

where $Z = \text{Tr}_A e^{-\beta H}$ is the partition function for the initial nucleus, H is the many-body hamiltonian, and the trace is over all states of the initial nucleus. The quantities $(\beta - \tau - \tau')$ and τ play the role of the inverse temperature in the parent and daughter nucleus respectively. A spectral expansion of ϕ shows that large values of these parameters guarantee cooling to the parent and daughter ground states. In these limits, we note that $\phi(\tau, \tau' = 0)$ approaches $e^{-\tau Q} |M_c|^2$, where $Q = E_i^0 - E_f^0$ is the energy release, so that a calculation of $\phi(\tau, 0)$ leads directly to the closure matrix element. If we then define

$$\eta(T, \tau) \equiv \int_0^T d\tau' \phi(\tau, \tau') e^{-\tau' Q/2}, \quad (41)$$

and

$$M^{2\nu}(T, \tau) \equiv \frac{\eta(T, \tau) M_c^*}{\phi(\tau, 0)}, \quad (42)$$

it is easy to see that in the limit of large τ , $(\beta - \tau - \tau')$, and T , $M^{2\nu}(T, \tau)$ becomes independent of these parameters and is equal to the matrix element in Eq. (37).

In the first applications, Radha *et al.* calculated the 2ν matrix elements for ^{48}Ca and ^{76}Ge [48]. The first nucleus allowed a benchmarking of the SMMC method against direct diagonalization. A large-basis shell

model calculation for ^{76}Ge has long been waited for, as ^{76}Ge is one of the few nuclei where the $2\nu\beta\beta$ decay has been measured precisely and the best limits on the 0ν decay mode have been established [49, 50, 51].

To monitor the possible uncertainty related to the g -extrapolation in the calculation of the 2ν matrix element for ^{76}Ge , SMMC studies have been performed for two quite different families of sign-problem-free hamiltonians ($\chi = \infty$ and $\chi = 4$). The calculation comprises the complete $(0f_{5/2}, 1p, 0g_{9/2})$ model space, which is significantly larger than in previous shell model studies [52]. The adopted effective interaction is based on the Paris potential and has been constructed for this model space using the Q -box method developed by Kuo [53].

As is shown in Fig. 3.3, upon linear extrapolation, both families of hamiltonians predict a consistent value for the 2ν matrix element of ^{76}Ge . The results $M^{2\nu} = 0.12 \pm 0.07$ and $M^{2\nu} = 0.12 \pm 0.06$ are only slightly lower than the experimental values ($M^{2\nu} = 0.22 \pm 0.01$ [51]). This comparison, however, should not be overinterpreted, as the detailed reliability of the effective interaction is still to be checked.

It is interesting that the closure matrix element found in the SMMC calculation and the average energy denominator ($M_c = -0.36 \pm 0.37$, $\bar{E} = -3.0 \pm 3.3$ MeV and $M_c = 0.08 \pm 0.17$, $\bar{E} = 0.57 \pm 1.26$ MeV for the two families of hamiltonians with $\chi = \infty$ and $\chi = 4$, respectively) are both significantly smaller than had been assumed previously. This is confirmed by a recent truncated diagonalization study [54].

3.4 γ -soft nuclei

Nuclei with mass number $100 \leq A \leq 140$ are believed to have large shape fluctuations in their ground states. Associated with this softness are spectra with an approximate $O(5)$ symmetry and bands with energy spacings intermediate between rotational and vibrational. In the geometrical model these nuclei are described by potential energy surfaces with a minimum at $\beta \neq 0$ but independent of γ [55]. Some of these nuclei have been described in terms of a quartic five-dimensional oscillator [56]. In the Interacting Boson Model (IBM) they are described by an $O(6)$ dynamical symmetry [57, 58, 59]. In the following we review the first fully microscopic calculations for soft nuclei with $100 \leq A \leq 140$ [60].

For the two-body interaction we used a monopole ($J = 0$) plus quadrupole ($J = 2$) force [61] supplemented by a collective quadrupole

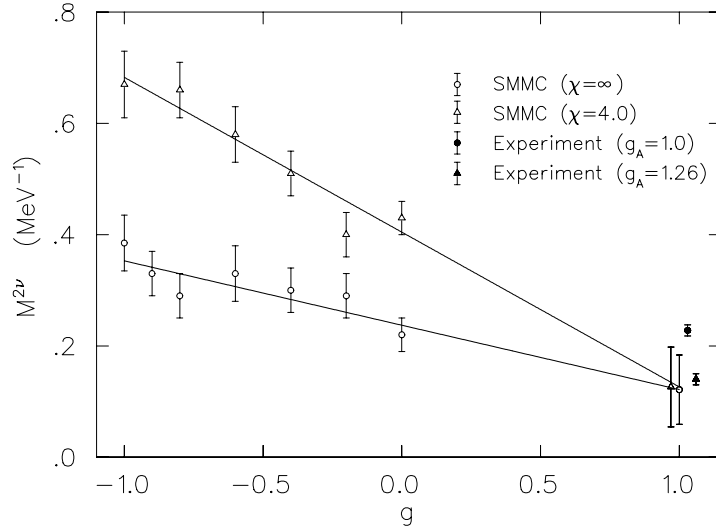


FIG 3.3. The 2ν matrix element for ^{76}Ge calculated within SMMC studies based on two families of hamiltonians which are free of sign problems. The physical values are obtained by linear extrapolation to $g = 1$. The experimental value for this matrix element [51] is indicated by the diamond (from [48]).

interaction:

$$H_2 = - \sum_{\lambda\mu} \frac{\pi g_\lambda}{2\lambda + 1} P_{\lambda\mu}^\dagger P_{\lambda\mu} - \frac{1}{2} \chi : \sum_{\mu} (-)^\mu Q_\mu Q_{-\mu} : , \quad (43)$$

where $::$ denotes normal ordering. The single particle energies and the other parameters were determined as described in Ref. [60].

We begin discussion of our results with the probability distribution of the quadrupole moment. This is obtained from the shape of each Monte Carlo sample, including the quantum-mechanical fluctuations through the variance of the Q operator for each sample, $\Delta_\sigma^2 = \text{Tr}(Q^2 U_\sigma) / \text{Tr}(U_\sigma) - \langle Q \rangle_\sigma^2$. The shape distribution $P(\beta, \gamma)$ can be converted to a free energy surface as discussed in Ref. [60].

The shape distributions of ^{128}Te and ^{124}Xe are shown in Fig. 3.4 at different temperatures. These nuclei are clearly γ -soft, with energy minima at $\beta \sim 0.06$ and $\beta \sim 0.15$, respectively. Energy surfaces calculated with Strutinsky-BCS using a deformed Woods-Saxon potential [62] also indicate γ -softness with values of β comparable to the SMMC values. These calculations predict for ^{124}Xe a prolate minimum with $\beta \approx 0.20$ which is lower than the spherical configuration by 1.7 MeV but is only 0.3 MeV below the oblate saddle point, and for ^{128}Te a shallow oblate minimum with $\beta \approx 0.03$. These γ -soft surfaces are similar to those obtained in the $O(6)$ symmetry of the IBM, or more generally when the hamiltonian has mixed $U(5)$ and $O(6)$ symmetries but a common $O(5)$ symmetry. In the Bohr hamiltonian, an $O(5)$ symmetry occurs when the collective potential energy depends only on β [55]. The same results are consistent with a potential energy $V(\beta)$ that has a quartic anharmonicity [56], but with a negative quadratic term that leads to a minimum at finite β .

The total E2 strengths were estimated from $\langle Q^2 \rangle$ where $Q = e_p Q_p + e_n Q_n$ is the electric quadrupole operator with effective charges of $e_p = 1.5e$ and $e_n = 0.5e$, and $B(E2; 0_1^+ \rightarrow 2_1^+)$ determined by assuming that most of the strength is in the 2_1^+ state. Values for $B(E2; 0_1^+ \rightarrow 2_1^+)$ of 663 ± 10 , 2106 ± 15 , and $5491 \pm 36 e^2 \text{fm}^4$ were found, to be compared with the experimental values [63] of 1164, 3910, and 9103 $e^2 \text{fm}^4$ for ^{124}Sn , ^{128}Te , and ^{124}Xe , respectively. Thus, the SMMC calculations reproduce the correct qualitative trend. The 2_1^+ excitation energies were also calculated from the E2 response function. The values of 1.12 ± 0.02 , 0.96 ± 0.02 , and 0.52 ± 0.01 MeV are in close agreement with the experimental values of 1.2, 0.8, and 0.6 MeV for ^{124}Sn , ^{128}Te , and ^{124}Xe , respectively.

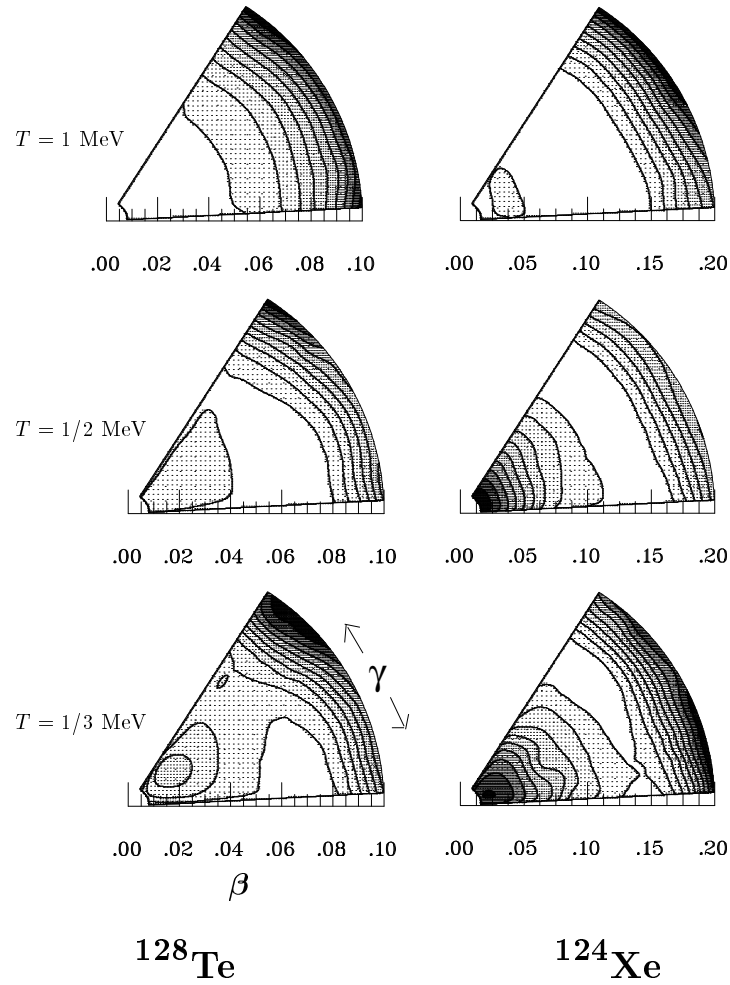


FIG 3.4. Contours of the free energy (as described in the text) in the polar-coordinate $\beta - \gamma$ plane for ^{128}Te and ^{124}Xe . Contours are shown at 0.3 MeV intervals, with lighter shades indicating the more probable nuclear shapes (from [60]).

Another indication of softness is the response of the nucleus to rotations, probed by adding a cranking field ωJ_z to the hamiltonian and examining the moment of inertia as a function of the cranking frequency ω . For a soft nucleus one expects a behavior intermediate between a deformed nucleus, where the inertia is independent of the cranking frequency, and the harmonic oscillator, where the inertia becomes singular. This is confirmed in Fig. 3.4 which shows the moment of inertia \mathcal{I}_2 for ^{124}Xe and ^{128}Te as a function of ω , and indicates that ^{128}Te has a more harmonic character. The moment of inertia for $\omega = 0$ in both nuclei is significantly lower than the rigid body value ($\approx 43\hbar^2/\text{MeV}$ for $A = 124$) due to pairing correlations.

Also shown in Fig. 3.4 are $\langle Q^2 \rangle$ where Q is the mass quadrupole, the BCS-like pairing correlation $\langle \Delta^\dagger \Delta \rangle$ for the protons and $\langle J_z \rangle$ (neutron pairing is less affected, and therefore not shown). Notice that the increase in I_2 as a function of ω is strongly correlated with the rapid decrease of pairing correlations and that the peaks in I_2 are associated with the onset of a decrease in collectivity (as measured by $\langle Q^2 \rangle$). This suggests band crossing along the yrast line associated with pair breaking and alignment of the quasi-particle spins at $\omega \approx 0.2$ MeV ($\langle J_z \rangle \approx 7\hbar$) for ^{128}Te and $\omega \approx 0.3$ MeV ($\langle J_z \rangle \approx 11\hbar$) for ^{124}Xe . The results are consistent with an experimental evidence of band crossing in the yrast sequence of ^{124}Xe around spin of $10 \hbar$ [64]. The alignment effect is clearly seen in the behavior of $\langle J_z \rangle$ at the lower temperature, which shows a rapid increase after an initial moderate change. Deformation and pairing decrease also as a function of temperature.

The total number of J -pairs ($n_J = \sum_\alpha n_{\alpha J}$) in the various pairing channels was also calculated. Since the number of neutrons in ^{124}Xe is larger than the mid-shell value, they are treated as holes. For $J = 0$ and $J = 2$, one can compare the largest $n_{\alpha J}$ with the number of s and d bosons obtained from the $O(6)$ limit of the IBM. For ^{124}Xe the SMMC (IBM) results in the proton-proton pairing channel are 0.85 (1.22) s ($J = 0$) pairs, and 0.76 (0.78) d ($J = 2$) pairs, while in the neutron-neutron channel we find 1.76 (3.67) s pairs and 2.14 (2.33) d pairs. For the protons the SMMC d to s pair ratio 0.89 is close to its $O(6)$ value of 0.64. However, the same ratio for the neutrons, 1.21, is intermediate between $O(6)$ and $SU(3)$ (where its value is 1.64) and is consistent with the neutrons filling the middle of the shell. The total numbers of s and d pairs—1.61 proton pairs and 3.8 neutron (hole) pairs—are below the IBM values of 2 and 6, respectively.

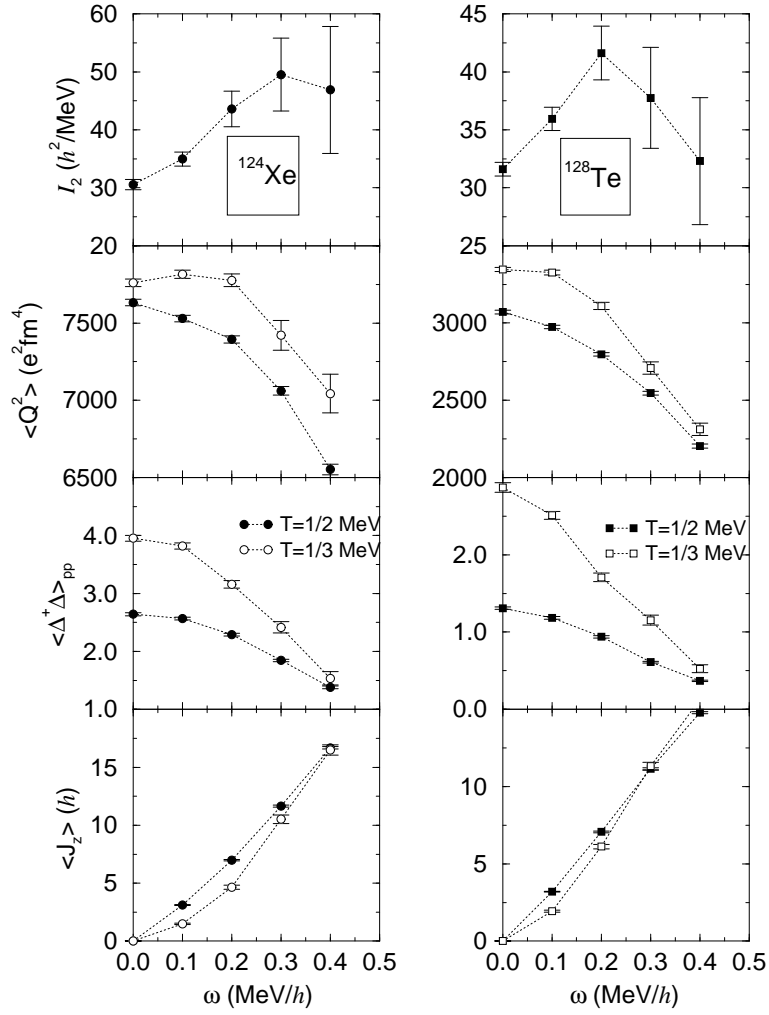


FIG 3.4 Observables for ^{124}Xe and ^{128}Te as a function of cranking frequency ω and for two temperatures. I_2 is the moment of inertia, Q is the mass quadrupole moment, Δ is the $J = 0$ pairing operator, and J_z is the angular momentum along the cranking axis (from [60]).

4 Illustrative calculations

4.1 Giant dipole resonances

To describe the GDR in ^{16}O , the $0p\text{-}1s0d\text{-}0f_{7/2}$ shell model space was used [65], and the residual interaction was composed of pairing and multipole terms with the specific parametrization given in [65],

$$V_{\text{res}} = \chi_1(q_p^1 - q_n^1)^2 + \chi_2(q_p^2 + q_n^2)^2 + \chi_4(q_p^4 + q_n^4)^2 . \quad (44)$$

Shown in Fig. 4.1 are the results obtained for ^{16}O for the dipole transitions $D = 1/2(q_p^1 - q_n^1)$ at temperatures $T = 0.5, 1.0, \text{ and } 2.0$ MeV. Although these calculations require further refinement, some general remarks are warranted. First, from the values of $R(\tau)$ at $\tau = 0$, the total dipole strength is roughly constant as a function of temperature, as is the first moment of the strength function. The width, or second moment, cannot be reliably extracted from the calculations presented in Fig. 4.1 due to large Monte Carlo errors. Still, the calculations are representative of what may be obtained with more samples (yielding smaller errors). A future study will involve a more complete model space description, and implementation of matrix-multiply stabilization so that lower temperatures may be studied.

4.2 Multi-major shell calculations

Numerous problems in nuclear physics would benefit from the ability to calculate shell model observables in more than a single oscillator shell. For example, the structure of light neutron-rich nuclei in the sd -shell requires inclusion of fp -shell orbitals in order to properly describe their deformation and cross shell characteristics. Experimentally, this region will be probed to understand the nature of weakly bound systems, and the response of nuclei near the neutron drip line to various physical probes. Multi- $\hbar\omega$ SMMC calculations should be no more difficult computationally than the $0\hbar\omega$ calculations that are now routine, although they do require increased memory and computational cycles.

When more than one oscillator shell is included, a new complication arises: excitations of the center-of-mass (CM) become mixed into the real nuclear excitations. This leads to spurious components of wave functions being incorporated into the calculations of observables. We have investigated two methods of removing these spurious components in the SMMC. Projecting out these components leads to another sign problem and has proven unworkable. The Gloeckner-Lawson prescription [66] has

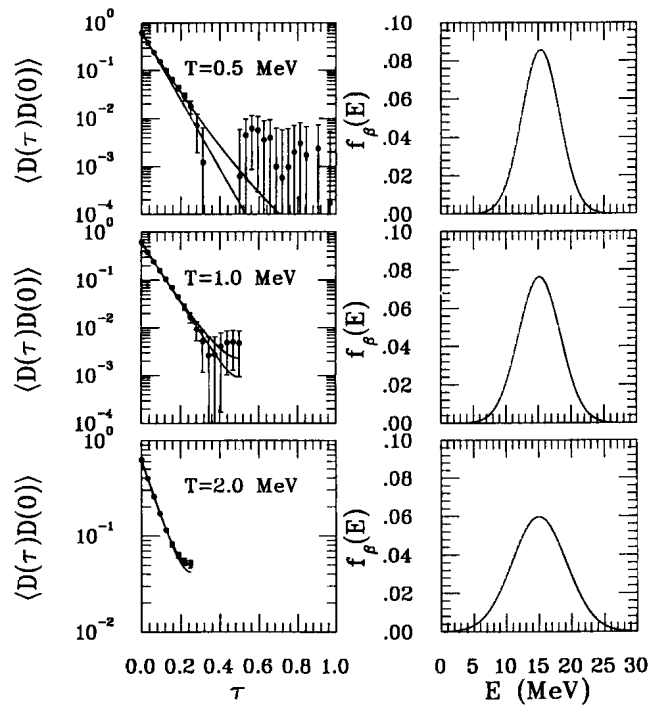


FIG 4.1 Response function (left panels) and their excitation strength distributions (right panels) for isovector dipole transitions in ^{16}O at $T = 0.5, 1.0,$ and 2.0 MeV.

been shown to work for fairly small CM multipliers (< 5) in comparisons with direct diagonalization calculations. Unfortunately, this method requires a “complete” $n\hbar\omega$ space to be fully effective and SMMC methods cannot work in such a complete space [67]. The Gloeckner-Lawson prescription will still remove the spurious solutions at the cost of also slightly affecting the non-spurious solutions. The best value of the multiplier is currently being investigated. Values of order 1 seem to be best.

Our current research focuses on the $N = 20$ and 28 shell closures for very neutron-rich nuclei where we may investigate how exact the shell closure really is for nuclei such as ^{32}Mg and ^{46}Ar . (In the *sdfp* shell this calculation allows excitations of up to $16\hbar\omega$ for ^{32}Mg .) Experimentally, ^{32}Mg is highly deformed [68]. An *sd*-shell calculation gives roughly 30% of this deformation, while the inclusion of the *pf*-shell yields much of the remaining deformation due to two-particle excitations into the *pf*-shell. There is no well-established interaction for the *sdpf* shell, so we have chosen to use the WBMB interaction of Ref. [69]. In order to find agreement with the experimental mass excess the single particle energies of the *pf* shell were lowered by 4 MeV relative to the *sd* shell. We are interested in both the deformation of ^{32}Mg , and the neutron-rich sulfur isotopes which have recently been experimentally measured[70]. In Fig. 4.2 we show for several nuclei in the region, the calculated mass excess for this interaction compared to experiment. We also show the total calculated $B(E2)$ vs. the experimentally measured $B(E2)$ to the first 2^+ state. The final panel shows the expectation value of the center-of-mass hamiltonian. For all of the nuclei, a spurious $2\hbar\omega$ solution would have $\langle H_{\text{CM}} \rangle \approx 20$ MeV. The center-of-mass contamination is seen to be quite small.

5 Concluding remarks

We have demonstrated in the preceding two sections the powers and limitations of the SMMC technique in describing nuclear properties. The SMMC technique, while often non-trivial to apply to a given situation, indeed sheds light on various aspects of nuclear systems. The most important studies mentioned above include the quenching of the Gamow-Teller strength, thermal and rotational properties of pair correlations, and the evolution of nuclear shapes with temperature.

We have witnessed enormous computational advances in the last several years. Large-scale parallel computing for scientific problems contin-

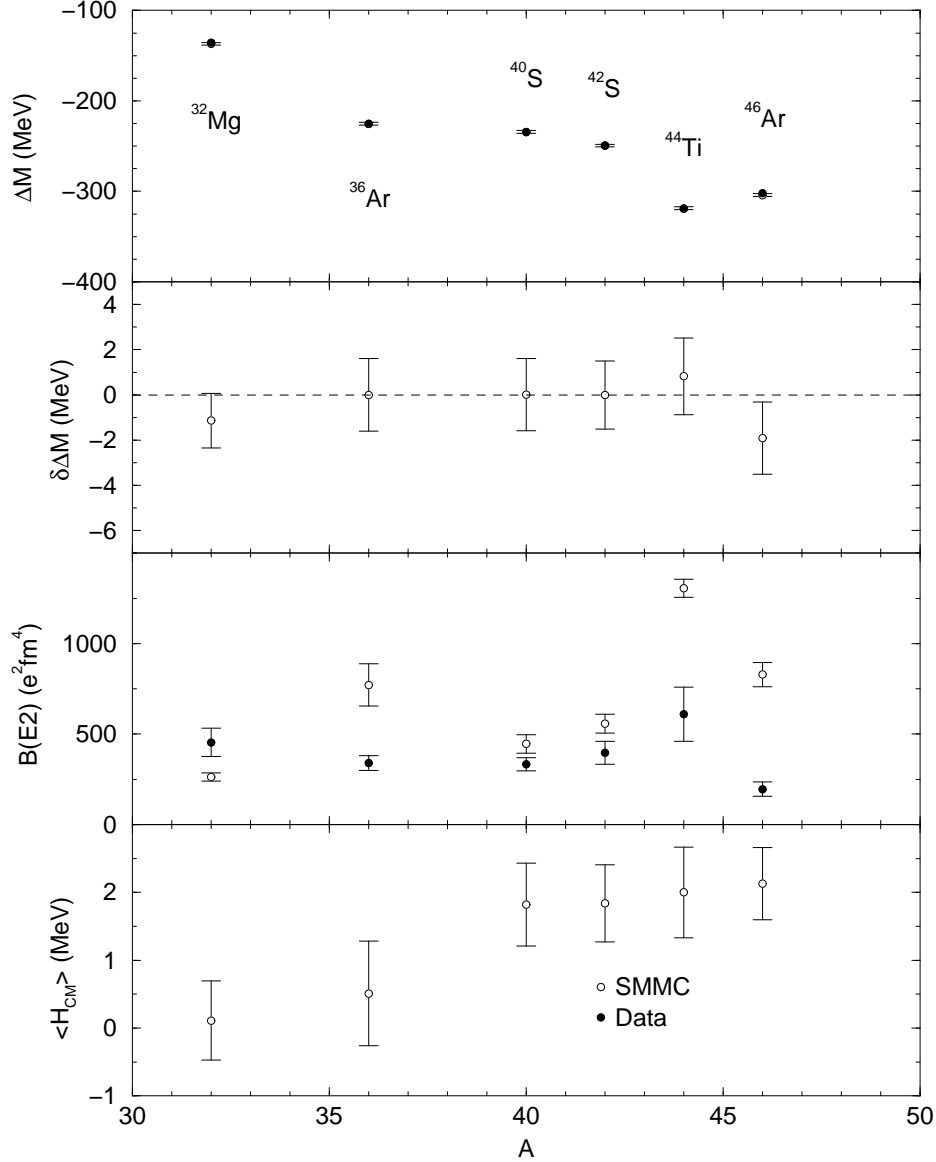


FIG 4.2 A selection of SMMC calculated observables vs experiment. A) The calculated and experimental mass excess. B) Deviation between experimental and calculated masses. C) The total calculated $B(E2)$ vs. the experimentally measured $B(E2)$ to the first excited 2^+ state. D) The expectation value of the center of mass hamiltonian. The values are much smaller than $2\hbar\omega$, the minimum value for a spurious wave function.

ues to move forward quickly. Thus some of the more difficult problems that have not been treated by SMMC at present could be pursued in the near future. Among these is the GDR in a several $\hbar\omega$ space; studies of nuclei in the *Pb* region; studies of weakly bound systems; and studies at very low temperatures [requiring matrix-multiply stabilization discussed in Ref. [18]]. The low temperature studies would allow for a detailed description of strength functions not currently available to us. The advent of radioactive beam experiments will also allow for interesting new physics to be studied within the realm of the shell model.

The ground state and thermal properties of nuclear matter are another intriguing application of SMMC methods. One approach is to use single particle states that are plane waves with periodic boundary conditions, and a *G*-matrix derived from a realistic inter-nucleon interaction; the formalism and algorithms we have presented here are then directly applicable. An alternative approach is to work on a regular lattice of sites in coordinate space and employ Skyrme-like effective interactions that couple neighboring sites; the calculation is then similar to that for the Hubbard model for which special techniques must be used to handle the large, sparse matrices involved [21]. Both approaches are currently being pursued.

Otsuka and collaborators [71] have recently proposed a hybrid scheme whereby some of the SMMC sampling methods are used to select a many-body basis, which is then employed in a conventional diagonalization. The brunt of their effort involves finding the local Hartree-Fock minima of the system, and then sampling around those minima. *J*-projection is approximately incorporated. With this approach one is able to obtain the lowest few discrete levels and transitions. The method is a way of truncating the many-body basis before diagonalization, and is thus complementary to SMMC in the same way as the conventional shell model.

The work discussed above is the culmination of the efforts of many people including Y. Alhassid, C. Johnson, G. Lang, E. Ormand, P.B. Radha, P. Vogel, and more recently M.T. Ressel, and J. White. This work was supported in part by the National Science Foundation, Grant Nos. PHY94-12818 and PHY94-20470. Oak Ridge National Laboratory (ORNL) is managed by Lockheed Martin Energy Research Corp. for the U.S. Department of Energy under contract number DE-AC05-96OR22464. DJD acknowledges an E.P. Wigner Fellowship from ORNL. Computational resources were provided by the Center for Advanced Computational Research at Caltech, the Maui High Performance Computing Center, The RIKEN computer center, and Center for Computational Sciences

at ORNL.

References

- [1] M.G. Meyer, Phys. Rev. **75** (1949) 1968; O.J. Haxel, J.H.D. Jensen and H.E. Suess, Phys. Rev. **75** (1949) 1766
- [2] J. Friedrich, P.G. Reinhard, Phys. Rev. **C33** (1986) 335.
- [3] J. Dobaczewski, W. Nazarewicz, T.R. Werner, J.F. Berger, C.R. Chinn, and J. Decharge Phys. Rev. **C33**, 2809 (1996)
- [4] P.G. Reinhard and C. Toepffer, Int. J. of Mod. Phys. **E3**, suppl. (1994).
- [5] S. Cohen and D. Kurath, Nucl. Phys. **73** (1965) 1; **A141** (1970) 145; D. Kurath, Phys. Rev. **C7** (1973) 1390; D. Kurath and D.J. Millener, Nucl. Phys. **A238** (1975) 269
- [6] B.H. Wildenthal, Prog. Part. Nucl. Phys. **11** (1984) 5; B.A. Brown and B.H. Wildenthal, Ann. Rev. Nucl. Part. Sci. **38** (1988) 29.
- [7] J.B. French, E.C. Halbert, J.B. McGrory, and S.S.M. Wong, Adv. Nucl. Phys. **3** (1969) 193; E.C. Halbert, J.B. McGrory, B.H. Wildenthal, and S.P. Pandya, Adv. Nucl. Phys. **4** (1971) 375
- [8] T.T.S. Kuo and G.E. Brown, Nucl. Phys. **85** (1966) 40; T.T.S. Kuo, Ann. Rev. Nucl. Sci. **24** (1974) 101
- [9] A. Poves and A.P. Zuker, Phys. Rep. **70** (1981) 235
- [10] see for example R.R. Whitehead, A. Watt, B.J. Cole and L. Morrison, Adv. Nucl. Phys. **9** (1977) 123
- [11] B. H. Wildenthal, in *Shell Model and Nuclear Structure: where do we stand?*, 2nd International Spring Seminar on Nuclear Physics, edited by A. Covello (World Scientific, 1988).
- [12] E. Caurier, A.P. Zuker, A. Poves and G. Martinez-Pinedo, Phys. Rev. **C50** (1994) 225; G. Martinez-Pinedo, A.P. Zuker, A. Poves and E. Caurier, Phys. Rev. **C55** (1997) 187.
- [13] E. Caurier, G. Martinez-Pinedo, A. Poves and A.P. Zuker, Phys. Rev. **C52** (1995) R1736

- [14] C.W. Johnson, S.E. Koonin, G.H. Lang and W.E. Ormand, Phys. Rev. Lett. **69** (1992) 3157
- [15] G.H. Lang, C.W. Johnson, S.E. Koonin and W.E. Ormand, Phys. Rev. **C48** (1993) 1518
- [16] W.E. Ormand, D.J. Dean, C.W. Johnson, G.H. Lang and S.E. Koonin, Phys. Rev. **C49** (1994) 1422
- [17] Y. Alhassid, D.J. Dean, S.E. Koonin, G.H. Lang and W.E. Ormand, Phys. Rev. Lett. **72** (1994) 613
- [18] S.E. Koonin, D.J. Dean, and K. Langanke, Phys. Repts. **278** (1996) 1.
- [19] J. Hubbard, Phys. Lett. **3** (1959) 77; R.D. Stratonovich, Dokl. Akad. Nauk., SSSR **115** (1957) 1907 [transl: Soviet Phys. Kokl. **2** (1958) 416]
- [20] G. Sugiyama and S.E. Koonin, Ann. Phys. **168** (1986) 1
- [21] W. von der Linden, Phys. Rep. **220** (1992) 53, and references therein.
- [22] J. E. Hirsch, Phys. Rev. **B28** (1983) 4059
- [23] N. Metropolis, A. Rosenbluth, M. Rosenbluth, A. Teller and E. Teller, J. Chem. Phys. **21** (1953) 1087
- [24] E.Y. Loh Jr., and J.E. Gubernatis, *Electronic Phase Transitions*, ed by W. Hanke and Yu.V. Kopaev (1992) 177
- [25] W.A. Richter, M.G. Vandermerwe, R.E. Julies, and B.A. Brown, Nucl. Phys. **A523** (1991) 325
- [26] K. Langanke, D.J. Dean, P.B. Radha, Y. Alhassid, and S.E. Koonin, Phys. Rev. **C52** (1995) 718
- [27] A. Nowacki, Ph.D. Thesis, Madrid, Spain, 1995
- [28] D.J. Dean, S.E. Koonin, K. Langanke, W. Nazarewicz, A. Nowacki, and A. Poves, in preparation (1997).
- [29] H.A. Bethe, Rev. Mod. Phys. **62** (1990) 801
- [30] M. B. Aufderheide, I. Fushiki, S. E. Woosley, and D. H. Hartmann, Astrophys. J. Suppl. 91 (1994) 389

- [31] G.M. Fuller, W.A. Fowler and M.J. Newman, ApJS **42** (1980) 447; **48** (1982) 279; ApJ **252** (1982) 715; **293** (1985) 1
- [32] A.L. Williams *et al.*, Phys. Rev. **C51** (1995) 1144
- [33] W.P. Alford *et al.*, Nucl. Phys. **A514** (1990) 49
- [34] M.C. Vetterli *et al.*, Phys. Rev. **C40** (1989) 559
- [35] S. El-Kateb *et al.*, Phys. Rev. **C49** (1994) 3129
- [36] T. Rönquist *et al.*, Nucl. Phys. **A563** (1993) 225
- [37] G.F. Bertsch and I. Hamamoto, Phys. Rev. **C26** (1982) 1323
- [38] M. Ericson, A. Figureau and C. Thevenet, Phys. Lett. **45B** (1973) 19; E. Oser and M. Rho, Phys. Rev. Lett. **42** (1979) 47; I.S. Townes and F.C. Khanna, Phys. Rev. Lett. **42** (1979) 51; A. Bohr and B. Mottelson, Phys. Lett. **100B** (1981) 10
- [39] M.B. Aufderheide, S.D. Bloom, D.A. Resler and G.J. Mathews, Phys. Rev. **C47** (1993) 2961; Phys. Rev. **C48** (1993) 1677
- [40] K. Langanke, D.J. Dean, P.B. Radha, and S.E. Koonin, Nucl. Phys. **A602** (1996) 244
- [41] K. Langanke, D.J. Dean, S.E. Koonin and P.B. Radha, Nucl. Phys. **A613** (1997) 253.
- [42] J. Engel, K. Langanke and P. Vogel, Phys. Lett. (December 1996)
- [43] D. Rudolph *et al.*, Phys. Rev. Lett. **76** (1996) 376
- [44] D.J. Dean, S.E. Koonin, K. Langanke, and P.B. Radha, Phys. Lett. B, in press (1997)
- [45] D.J. Dean, S.E. Koonin, K. Langanke, P.B. Radha, and Y. Alhassid, Phys. Rev. Lett. **74**, (1995) 2909
- [46] J.J. Cowan, F.-K. Thielemann and J.W. Truran, Physics Rep. **208** (1991) 267
- [47] D.C. Zheng, unpublished
- [48] P.B. Radha, D.J. Dean, S.E. Koonin, T.T.S. Kuo, K. Langanke, A. Poves, J. Retamosa and P. Vogel, Phys. Rev. Lett. **76** (1996) 2642

- [49] A.A. Vasenko *et al.*, Mod. Phys. Lett. **A5** (1990) 1229
- [50] F.T. Avignone *et al.*, Phys. Lett. **B256** (1991) 559
- [51] M. Beck *et al.*, Phys. Rev. Lett. **70** (1993) 2853; A. Balysh *et al.* Phys. Lett. **B322** (1994) 176
- [52] W.C. Haxton and G.J. Stephenson Jr., Prog. in Part. and Nucl. Phys. **12** (1984) 409
- [53] T.T.S. Kuo and E. Osnes, *Lecture Notes in Physics* **364** (Springer-Verlag, Berlin, 1990) 1
- [54] E. Caurier, F. Nowacki, A. Poves and J. Retamosa, preprint (Universite Louis Pasteur, Strasbourg; Universidad Autonoma de Madrid (January 1996)
- [55] L. Willets and M. Jean, Phys. Rev. **102** (1956) 788
- [56] O.K. Vorov and V.G. Zelevinsky, Nucl. Phys. A **439** (1985) 207
- [57] F. Iachello and A. Arima, *The Interacting Boson Model* (Cambridge University Press, Cambridge, 1988)
- [58] W. Krips *et al.*, Nucl. Phys. A **529** (1991) 485
- [59] T. Otsuka, Nucl. Phys. A **557** (1993) 531c
- [60] Y. Alhassid, G.F. Bertsch, D.J. Dean, and S.E. Koonin, Phys. Rev. Lett. **77** 1444 (1996).
- [61] R. Broglia, D.R. Bes and B.S. Nilsson, Phys. Lett. B **50** (1974) 213
- [62] R. Wyss and W. Nazarewicz, private communication.
- [63] S. Raman *et al.*, Atomic Data and Nuclear Data Tables **36** (1987) 1
- [64] W. Gast *et al.*, Z. Phys. A **318** (1984) 123
- [65] W.E. Ormand, Nucl. Phys. **A569**, 63c (1994).
- [66] D.H. Gloeckner and R.D. Lawson, Phys. Lett. **53B**, 313 (1974)
- [67] J.B. McGrory and B.H. Wildenthal, Phys. Lett. **B60**, 5 (1975)
- [68] T. Motobayashi, *et al.*, Phys. Lett. **B346**, 9 (1995)

- [69] E.K. Warburton, J.A. Becker, and B.A. Brown, Phys. Rev. **C41**, 1147 (1990)
- [70] H. Scheit, *et al*, Phys. Rev. Lett. **77**, 3967 (1996)
- [71] M. Honwa, T. Mizusaki and T. Otsuka, Phys. Rev. Lett. **75** (1995) 1284

